Master of Science Thesis in Electrical Engineering
Department of Electrical Engineering, Linköping University, 2023

Predictive Control for Mitigating Solar Power Variations in Isolated Steam Power Systems

Rasmus Björk

Master of Science Thesis in Electrical Engineering

Predictive Control for Mitigating Solar Power Variations in Isolated Steam Power Systems

Rasmus Björk

LiTH-ISY-EX–23/5586–SE

Supervisor: **Daniel Jung**
ISY, Linköpings universitet
Carl Ressel
Solvina AB

Examiner: **Christofer Sundström**
ISY, Linköpings universitet

Division of Vehicular Systems
Department of Electrical Engineering
Linköping University
SE-581 83 Linköping, Sweden

Abstract

The need to reduce the amount of fossil fuel consumed by industry is vital. However, it is crucial to understand that industry is less inclined to shift its consumption from fossil fuels to renewable energy sources solely based on environmental concerns; to realistically make industry switch from fossil fuels to renewable energy sources, renewable energy sources must provide efficient results for industry. An aspect of verifying the efficiency of solar power in an industrial setting is by studying how various control techniques can accommodate solar power alongside fossil fuels.

This thesis aims to analyze whether a predictive control model is suitable for supplying an industrial plant with solar power alongside its coal power. This thesis will study two main forms of predictive control: a PID controller featuring a feedforward component and MPC control.

The work within the thesis resulted in modelling an industrial plant, both physical and mathematical, and an optimization framework to test the MPC. The framework can be extended to include additional components as well as to introduce disturbances into the model.

The results of this thesis project prove that there are great improvements in performance when applying predictive features to control systems. The predictive control systems presented in this thesis decrease the usage of a buffer in the form of a battery - signifying economic advantages to the predictive methods, and decreasing the total generated power fluctuations by accommodating the incoming solar power before it enters the system.

Acknowledgments

I want to thank my two supervisors for their continuous support throughout this thesis. So, thank you Carl Ressel from Solvina AB and Daniel Jung from Linköping University. A special thanks to my friends who have made my university experience truly great.

Göteborg, May 2023
Rasmus Björk

Contents

1

Introduction

The urgency of transitioning from fossil fuels and embracing renewable energy sources cannot be overstated. The critical need to reduce our dependence on fossil fuels arises from the myriad environmental, economic, and social challenges that its usage presents. The environmental implications of continued reliance on fossil fuels are vast. By embracing renewable energy sources it is possible to harness nature's abundant and clean resources to minimize carbon emissions and mitigate the detrimental effects of climate change.

Increasing the use of renewable energy within a fossil fuel-dominated industry would be a great asset in the combatting of climate change. By studying the interaction between renewable energy sources and fossil fuels via industrial control systems, it will be assessed whether it is a viable energy transition strategy for the industry to make: it is an easier choice for the industry to transition to renewable energy if it improves the performance and efficiency of its workings; not solely if the transition is based on environmental concerns.

1.1 Background and purpose

Large industry complexes are often equipped with their own boilers and onsite turbines for generating electricity. This also allows the complex to disconnect from the national power grid and run the internal system as a localized power system. Following the desire to increase sustainability on-site solar panel solutions have been introduced. However, solar power generation puts new requirements on existing power production as a result of variations in solar power radiation.

The essence of the development is to optimize the use of solar power in contrast to the use of coal for fueling boilers to generate power. The optimization will be achieved by replacing the coal-based power with as much solar power as possible. The issue that arises is that the added solar photovoltaic system is a

fast-responding system while the coal-based power generation is slow; with a regular feedback control system, the industrial complex may experience downtime as clouds or other anomalies in the solar PV system reduces the produced solar power - leading to increased coal power generation which takes time to counteract the missing solar power.

Solvina AB is interested in developing a predictive control system to combat downtime. By predicting solar power variation, the objective is to feed information to the industrial complex before the actual loss in solar power occurs; thus yielding the boiler system adequate time to generate the anticipated power loss.

1.2 Related research

Kim et al. [19] compares a nonlinear model predictive control (NMPC) to a PID controller in controlling a heavy-duty gas turbine power plant for frequency and temperature control. The research showed that the NMPC provided better output responses with smaller settling times and less oscillatory behavior; additionally, the NMPC reacted more forcefully to changes and reacted better to large rapid changes than the PID controller.

By using solar-aided power generation, Han et al. [13] show that by using non-concentrating solar energy, the cost of electricity generation decreases. The process works by applying solar energy in the air preheating process which yields a decrease of 36.6% in the exergy loss.

Palma-Behnke et al. [26] introduce the concept of a rolling horizon strategy for energy management. The strategy involves optimizing a microgrid's energy management over a series of short time intervals. This approach allows for more accurate and timely decision-making, as it takes into account the real-time energy consumption and generation within the microgrid. The proposed microgrid energy management system (MEMS) consists of three main components: a forecasting model, an optimization model, and a control strategy. The forecasting model predicts the energy consumption and generation of the microgrid over the short-term horizon. The optimization model uses this forecast to determine the optimal energy dispatch strategy for the microgrid, considering various constraints such as the energy storage capacity and the maximum power output of renewable energy sources. Finally, the control strategy executes the optimal dispatch strategy in real time. The authors evaluate the performance of the proposed MEMS using a simulation model based on a real microgrid. The simulation results demonstrate that the proposed MEMS can effectively balance the energy supply and demand within the microgrid while minimizing the overall energy costs and ensuring system stability.

Bigarelli et al. [6] uses an MPC algorithm that takes into account a range of parameters, such as weather conditions, energy demand, and the characteristics of renewable energy sources. It then generates an optimal control strategy that minimizes the cost of energy production and consumption while meeting the energy demand requirements. The authors also use a hybrid MPC algorithm that combines both deterministic and stochastic models. The deterministic models

are used to predict energy production and consumption for the short term, while the stochastic models account for the uncertainties associated with weather conditions and energy demand.

Zhang et al. [29] uses a multi-rate MPC algorithm to account for differences in time scales between fast and slow systems. The MPC algorithm adapts the control input accordingly by using various prediction horizons depending on the systems' time scales. This approach yields an efficient structure to impose different dynamics on the controlled variables. Chen et al. [10] also uses an MPC controller accounting for both a fast- and slow-responding system. However, the authors, instead of studying various prediction horizons, approach the problem by applying a multi-rate sampling system. I.e., the authors use a faster sampling rate for the fast sub-system and a slower sampling rate for the slow sub-system.

McCloy et al. [24] propose an approach that utilizes a contraction analysis framework to capture the essential dynamics of a fast and slow sub-system. The authors compute contraction metrics to obtain valuable insights regarding the stability and performance of the sub-systems, which are then fed into the constraints of the MPC controller. The MPC controller applies these metrics to adapt the control input. They demonstrate the proposal by analyzing a chemical process with a fast and slow sub-system. The authors conclude that the contraction-constrained MPC method outperforms traditional MPC methods in terms of stability and performance.

A lot of the previous research on combining fossil fuels and solar energy is generally concerned with applying the solar energy to inherent processes within the boiler, i.e., pre-/re-heating the steam [25] [2] [3] [27] [8] [9]; and as such not a lot of previous research has been done on merging solar energy with the energy output of the boiler.

1.3 Problem formulation

The objective in this project is to develop a predictive controller for a plant consisting of a physical plant and incoming solar power. The controller should incorporate predictive elements in order to preemptively steer the system when solar power is approaching. Two predictive controllers are explored in this thesis project: a PID controller with a predictive feature and a Model Predictive Controller. Each controller is incorporated into the industrial complex model where it will be evaluated by how well it responds to incoming solar power.

1.4 Delimitation

There will be no hardware implementation in the thesis. The thesis is a simulated, software study where the performance of the predictive controller will be evaluated. Being a simulated study, many unknown real-world factors will not be considered.

Throughout the project, the reference input will be constant. The sole changing variable will be the solar input. The project will not consider other system

disturbances: i.e., measurement errors, system noise, and external interferences.

This thesis utilizes only necessary system parts and as such excludes non-vital components to create a streamlined and optimized model. By using only the vital system parts, the model's computational load is reduced, resulting in greater efficiency and fewer errors. This approach allows for the creation of a customized solution that fulfills specific requirements and achieves desired results.

1.5 Description of approach

The main modelling environment will be constructed in Dymola. This environment will contain the various parts of the industrial complex that are of significance in this thesis project. The environment will be based on Solvina's previous model of the industrial complex and the key features of significance will be extracted from said model.

Once the environment has been constructed it will be transferred to MATLAB where the predictive features and the control strategies will be implemented. The Dymola environment will split into blocks and be transferred to MATLAB. The control models will be created in MATLAB and the experimental setup will be in Simulink.

The solar prediction - fully customizable as the solar PV output is known - will be completely accurate: this is meant to prove a proof-of-concept that a predictive controller can improve power efficiency by reducing the amount of coal used.

1.6 Outline

In Chapter 2, the industrial complex is presented: how the complex works as a microgrid as well as the complex's parts and components. Chapter 3 notes the modelling necessary within the project. The modelling involves the turbines and generators, the battery, the coal boiler, and the solar PV. The modelling is necessary to make the simulation accurate towards the real plant and to yield realistic results. The control theory is presented in Chapter 4 and explores PID controllers, feedforward control, MPC, and constrained MPC. The PID and MPC controllers will be compared to the baseline industrial complex model. Chapter 5 presents the thesis' method: the evaluation of the control theory, an overview of the simulation setup, and how solar prediction and the controllers are implemented within the system. Chapter 6 discusses the results of applying the controllers compared to the baseline model. Chapter 7 concludes with a discussion of the project and future work related to the project.

2

Modelling of components

Various aspects of the system need to be modelled to complement the controllers. This involves modelling the turbine and generator, the battery, the coal boiler, and the solar photovoltaic. These models are presented in this chapter. The components will be modelled in Dymola and exported as an FMU block to make the components compatible with MATLAB. The Dymola plant involves graphical interfaces for the plant's dynamic physical relations. To model the MPC controller it is thus necessary to translate these dynamic physical relations to discrete mathematical formulas. The mathematical formulas will be modified to a sampling rate of 10 seconds to decrease the computational complexity in the optimization, while the Dymola model is sampled every 1 second. In the CMPC-solution, the PID controllers regulating the battery's charging and the coal input ratio have been removed. Instead, the PID controllers are replaced by control inputs that the optimizer can control to solve the optimization problem. Furthemore, a schematic model of the industrial complex will be presented.

2.1 Industrial complex

The industrial complex that is used as the case study in this master's thesis can be viewed as a microgrid. A microgrid is an autonomous grid where there does not need to be an interconnection to the main grid; as such a microgrid experiences a great decentralization and must be self-reliant in its energy domain. A microgrid generally features various energy sources - in recent times the discussion on microgrids is based on renewable energy sources - that cooperate to satisfy the microgrid's energy demands [16] [21] [14]. A microgrid generally involves both consumers of energy: electric vehicles, homes and facilities etc, and producers of energy: i.e., renewable energy sources and power generators, alongside various storage techniques and a connection/non-connection to the main utility grid.

The complete industrial complex is not of interest in this thesis; solely the components related to the solar power and the coal boiler in terms of the control system are of interest: as such no condensation process etc will be considered. A schematic outline of the industrial complex can be seen in Figure 2.1. The amount of coal needed to keep the baseline industrial model running, i.e., a model without solar power is denoted as r_{coal}. Once solar power enters the complex, the sum of w_{steam} and w_{sol} enters the load and an increase in the frequency f_{load} is expected. It is within this framework that the predictive controller will be used. By predicting when there will be an increase in solar power production, the coal input should respond accordingly and decrease the resulting w_{steam} before w_{sol} enters the system to not increase f_{load} and to therefore minimize the usage of the battery. If wrongly predicted, solar power could enter a system with a full battery and a load already met. In this case, the controller C_r must open the valve to decrease the pressure and consequently w_{steam} to not overload the frequency network. However, this will waste energy as power produced by the steam will leave the system.

There are four controllers in the complex: C_r which controls the release valve which releases steam if the pressure within the pipes exceeds a threshold; C_v controls the valve which throttles the steam which goes to the turbine - there is a maximum amount of steam that the turbine can handle at a given time; C_b regulates the frequency within the system. If the frequency is too high, it will use the excess power to charge the battery, if there is a deficit of energy in the system, it will discharge the battery; finally, C_r controls the ratio of coal that will enter the coal boiler. This is achieved by inspecting the battery's charge level and adjusting the ratio accordingly. Noteworthy for the process is that the battery's level of charge is the sole variable controlling the coal input; this is motivated by the following: if the battery is highly charged, this means that the loads' power requirements are met and that the system is approaching a high excess of energy, therefore the system requires less power input. Similarly, if the battery is low on charge, this means that the battery has been used to compensate for a deficit of energy within the system and that the boiler needs more power input for adjusting the deficit.

2.2 Turbine and generator

The inherent inertia of the turbine and the generator will be simulated by a rotating mass. The rotating mass symbolizes the inertia at the outset of running the turbine and the generator as well as the stored mechanical energy within the industrial complex; the rotating mass that controls the frequency has an inertia of 64092 $kg\ m^2$. It is within this component that the frequency is generated.

The frequency is generated by applying the net power entering the system to the rotating mass: the net power is the difference between the total watt generated and the system loads. Figure 2.2 shows how the net power enters the inertia model and how the generated frequency continues.

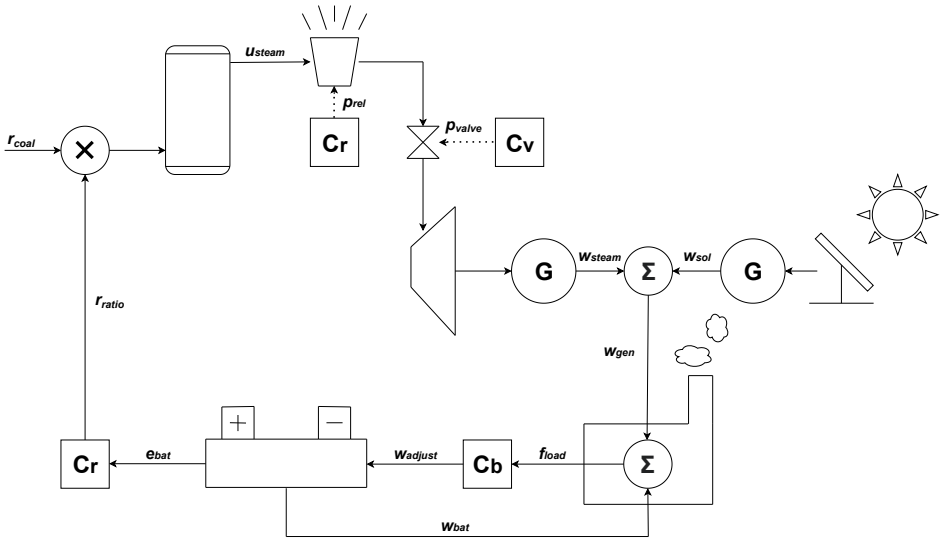

Figure 2.1: *Overview of the industrial complex.*

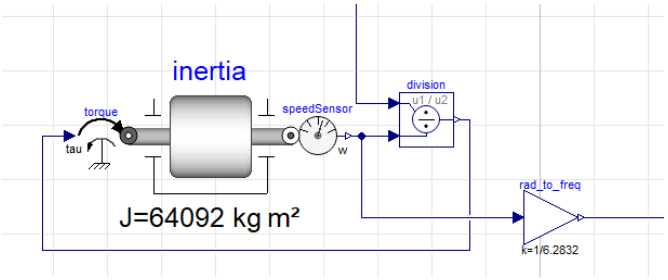

Figure 2.2: *Dymola model of the frequency generator.*

The system equation for the inertia is

$$J\dot{\omega}(t) = \tau(t) \tag{2.1}$$

where J is the moment of inertia, ω the angular velocity, and τ the torque. The torque can be re-written to

$$\tau(t) = \frac{P_{net}(t)}{\omega(t)} \tag{2.2}$$

where P_{net} is the net power. Modifying the equations to

$$\dot{\omega}(t) = \frac{P_{net}(t)}{J\omega(t)} \tag{2.3}$$

yields a function of the angular acceleration. The frequency at time $t + 1$ can

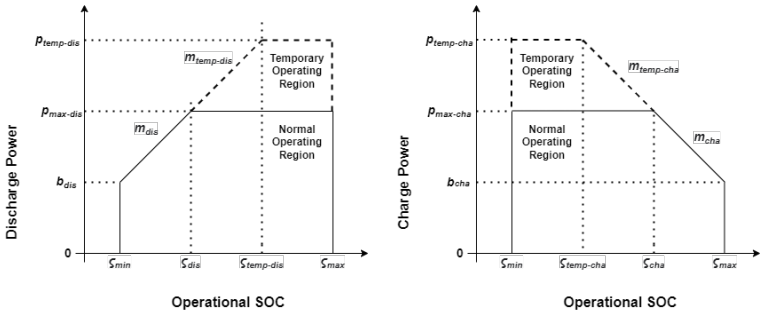

Figure 2.3: *Discharge power (left) and charge power (right) based on IEEE battery standard [17].*

therefore be calculated by

$$f(t+1) = f(t) + \frac{1}{(2\pi)^2}\frac{P_{net}(t)}{Jf(t)}. \tag{2.4}$$

For controller usage, the frequency generation model will be linearized. The linearization will be constructed around the operating point of 50 Hz as this is the frequency at which the system will operate while operating under the constraints. The linearization is made within the Dymola environment which yields a linearized model

$$f(n+1) = f(n) + K_{lin}\frac{1}{(2\pi)^2}t_s\Big(P_{tot}(n) - P_{load} - B(n)\Big) \tag{2.5}$$

where the linearization factor, $K_{lin} = 4.966 \cdot 10^{-8}$. The constant internal load of the industrial plant, P_{load}, is $2.44 \cdot 10^8$ Watt. $B(n)$ is the battery state of energy charging as modelled in Section 2.3.

2.3 Battery

The battery will be modelled congruent with IEEE standard [17]. IEEE standard divides a battery's operational SOC into discharge power and charge power and the operating regions for each mode can be viewed in Figure 2.3.

In essence, what is noteworthy is that the battery discharges slower at a lower state of charge and charges slower at a higher state of charge. The discharge power of the battery will be modelled as the following. ζ_{min}, i.e., the state of charge where the battery can start discharging the load, will be 0% of ζ_{max}; ζ_{dis} will be 10% of ζ_{max} which represents where the battery can discharge at maximum capacity. b_{dis}, the rate at which the discharge power commences, is set at 20% of $p_{max-dis}$. The rate at which the discharge power increases alongside the state of charge, m_{dis}, is linearly modelled as

$$m_{dis} = \frac{p_{max-dis} - b_{dis}}{\zeta_{dis} - \zeta_{min}} = \frac{0.8p_{max-dis}}{0.1\zeta_{max}}. \tag{2.6}$$

Similarly, for the charging power, the rate at which the charge power increases alongside the state of charge, is linearly modelled as

$$m_{cha} = \frac{-p_{max-cha} + b_{cha}}{\zeta_{max} - \zeta_{cha}} = -\frac{0.9p_{max-cha}}{0.2\zeta_{max}} \tag{2.7}$$

where ζ_{cha} is evaluated at $0.8\zeta_{max}$ and b_{cha} is set at 10% of $p_{max-cha}$. This creates the linear models for the rate of discharge and charge power

$$y_{cha} = p_{max} - \zeta^{'} \cdot \frac{0.9p_{max}}{0.2\zeta_{max}} \tag{2.8}$$

where

$$\zeta^{'} = \zeta - \zeta_{cha} \tag{2.9}$$

with ζ being the actual SOC, and

$$y_{dis} = b_{dis} + \zeta^{'} \cdot \frac{0.9p_{max}}{0.1\zeta_{max}} \tag{2.10}$$

where

$$\zeta^{'} = \zeta - \zeta_{min}. \tag{2.11}$$

The battery model will assume

$$m_{temp-dis} = m_{dis} \tag{2.12}$$

and

$$m_{temp-cha} = m_{cha} \tag{2.13}$$

with the temporary operating region at 110% capacity of the normal operating region such that

$$p_{temp-dis} = 1.1p_{max-dis} \tag{2.14}$$

and

$$p_{temp-cha} = 1.1p_{max-cha}. \tag{2.15}$$

The mathematical model of the battery's SOC is simply modelled through

$$SOC(n+1) = SOC(n) + t_s B(n) \tag{2.16}$$

where t_s is the sampling time and B the battery charging. From the IEEE standard of battery charging, the constraints on the battery charging is a function of the battery's SOC - $\zeta(SOC)$. The battery is modelled so that the maximum charge is at 10^{11} Ws which is the same as 28 MWh.

2.4 Coal boiler

The coal boiler is modelled using a first-order transfer function. A first-order transfer function model is built by a three-parameter model

$$G(s) = \frac{K_p}{1 + sT} e^{-sL} \tag{2.17}$$

where K_p is the steady-state gain, T the time constant, and L the time delay. The model is a non-physical, non-constrained, system where the system from coal input to watt generation is modelled. Experimental results yield the linear transfer function

$$\frac{3.35e8}{262s + 1} e^{-130s} \tag{2.18}$$

which represents the sub-system "coal input to watt generation". Figure 2.4 shows the results of the modelling where the red line is the watt generation of the actual system and the blue line is the watt generation of the modelled system. The initial condition of the experiment is non-zero which is why there is no inherent delay in the first step response. However, the second and third step responses show the 130 seconds time delay, as the step-responses activate at 2000 seconds and 3000 seconds respectively.

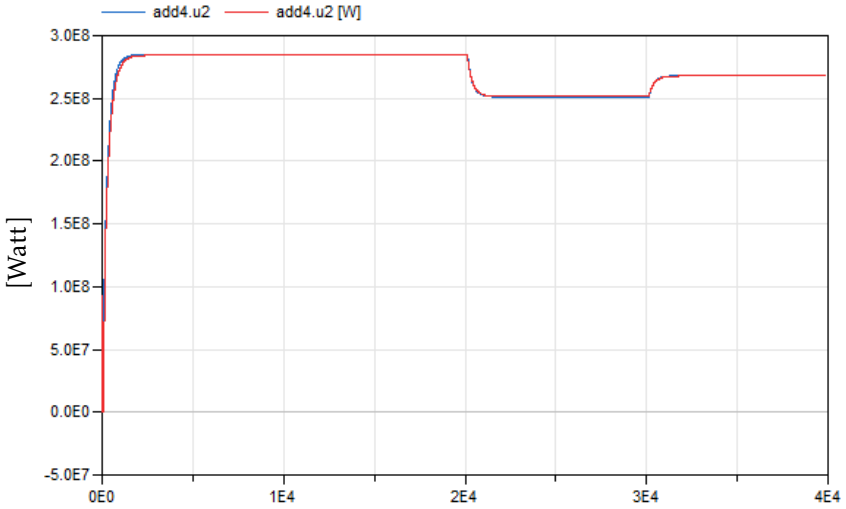

Figure 2.4: *Step response of the coal boiler and its model.*

The response from the steam generating system is known from (2.18). This response must also be discretized. This will be performed by the Tustin method which takes a continuous system and discretizes it based on a desired sampling time. The Tustin method converts a linear, time-invariant transfer function $H_a(s)$ to a discrete transfer function $H_d(z)$ by approximating the bilinear transformation from the s-plane to the z-plane to

$$s \leftarrow \frac{2}{t_s} \frac{z - 1}{z + 1} \tag{2.19}$$

which yields

$$H_d(z) = H_a(s)\Big|_{s=\frac{2}{t_s}\frac{z-1}{z+1}} = H_a(\frac{2}{t_s}\frac{z-1}{z+1}) \tag{2.20}$$

and transforms

$$H_a(s) = \frac{3.35 \cdot 10^8}{262s + 1} e^{-130s} \tag{2.21}$$

to

$$H_d(z) = \frac{1.255 \cdot 10^7}{z - 0.9626} z^{-13} \tag{2.22}$$

which can in turn be transformed to a first-order discrete-time system

$$P_s(n+1) = 0.9626 P_s(n) + 1.255 \cdot 10^7 u_c(n-13) \tag{2.23}$$

where u_c is the control input for the coal. There is thus a 13 time-step delay for the control input to affect the steam generation. The steam generation model has made simplifications in the real steam generation system; for instance, there is no PID controller for controlling the steam release valve, nor a PID controller for regulating the steam pressure entering the turbine. However, the simplification works as the inherent lower and upper bounds for steam production are set in order to constrain the system state within these viable bounds: the steam production will never reach values that would trigger the PID controllers to start regulating the steam pressure.

The control input for the coal generation, due to the system's inherent delay, have its first 13 coal input ratios bounded by the previous iteration's coal input ratio values - the delayed control inputs; as such they are simply modelled as

$$u_c(n) = u_{c_d}(n) \text{ for } n \in [1, 13]. \tag{2.24}$$

The other coal input ratio control inputs

$$u_c(n) \text{ for } n \in [14, p+1] \tag{2.25}$$

where p is the prediction horizon, are free to choose by the optimizer; note that it will take 13 time steps before these chosen control inputs will affect the steam generator.

2.5 Solar PV

As there are no current data on the solar PV:s that will be used within the industrial complex, Arzani et al. [4] analysis of commercial PV systems will be used to model the step-response of the solar PV complex. Arzani notes that the step response time of solar PV is on a scale between 0.2 and 4 seconds depending on the irradiance step change. This leads to a system in which the coal boiler is significantly slower responding than the solar PV. It is therefore clearly noticeable that the rapid-dynamic output of the solar PV:s cannot be compatible with the slow-dynamic coal boiler. The inherent characteristics of the coal boiler are too

slow to effectively react to the dynamically changing solar input and it is clear that the coal boiler controller needs to be modified.

The power generation's mathematical model for the MPC controller is steam power plus solar power, which is modelled as

$$P_{tot}(n) = P_s(n) + P_{sol}(n). \tag{2.26}$$

3

Control algorithms

Two control methods are presented in this chapter: a predictive PID-based controller with feedforward based on predicted solar radiance, and Model Predictive Control (MPC). Furthermore, an extension of MPC, constrained MPC (CMPC), is explored.

3.1 PID

The PID controller and its sub-variants are feedback control methods which are the *de facto* main control methods within the industry. Their versatility and ease of implementation make them a common choice for industrial applications. A PID controller is based on three sub-components: a proportional component, an integrating component, and a differential component with the three functions working in parallel. The equation for the PID controller is given by (3.1)

$$u(t) = K_P e(t) + K_I \int_0^t e(\tau)\, d\tau \; + K_D \frac{d}{dt} e(t) \tag{3.1}$$

where K_p, K_I, and K_D are tuning parameters reflecting the influence of each subcomponent.

A PID controller works by continuously monitoring the error between a desired set point and the actual process variable and adjusting the control output in proportion to the magnitude of this error. The proportional, integral, and derivative terms in the controller's algorithm each contribute to uniquely correcting the error, leading to a highly responsive and stable control system.

The proportional term provides a control output proportional to the current error, helping to correct for large and sudden changes in the process variable.

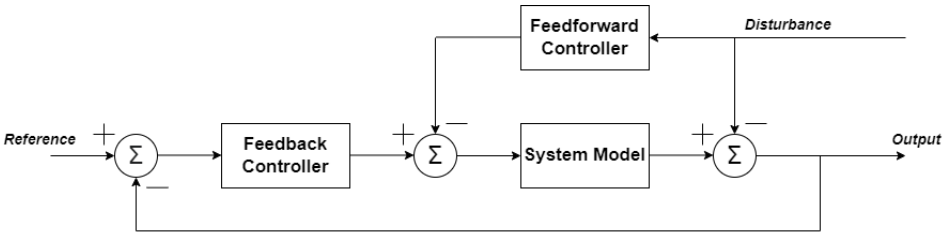

Figure 3.1: *Schematic model of a feedforward controller for disturbance rejection.*

The integral term accounts for the accumulated error over time, compensating for any persistent error that is not corrected by the proportional term. Finally, the derivative term uses the rate of change of the error to predict future errors and provide anticipatory control, smoothing out any overshoots or oscillations in the control output.

The ease of implementation of PID controllers is largely due to their simple and intuitive control algorithms, which can be implemented using basic mathematical operations and do not require complex or specialized hardware. Additionally, PID controllers can be easily tuned to perform optimally for a wide range of control applications.

3.2 Predictive control

In applying predictive control to counteract the issues presented in this project, there are two predictive methods that will be considered: applying feedforward control to the PID controller, and creating an MPC controller.

3.2.1 Feedforward control

Feedforward control is a control strategy that is often used in conjunction with PID control. It is a predictive control technique that uses a model of the system to predict the effect of changes in the system input on the system output. Feedforward control is often used for disturbance rejection. The goal of disturbance rejection is to eliminate disturbances as soon as they enter the system and not have to wait until the disturbance has traversed through the system, producing an error signal driving the feedback controller to react [22]. A schematic model of a feedforward controller can be viewed in Figure 3.1.

From the schematic model in Figure 3.1 it is easy to create a Laplace transform of the components and to create a closed-loop transfer function from disturbance to process output. First, however, consider the model as a Laplace transform where the output and disturbance are denoted $Y(s)$ and $D(s)$ respectively; the feedforward and feedback controllers as $F_f(s)$ and $F_b(s)$ respectively; and the system model as $G(s)$. The final closed-loop transfer function from disturbance

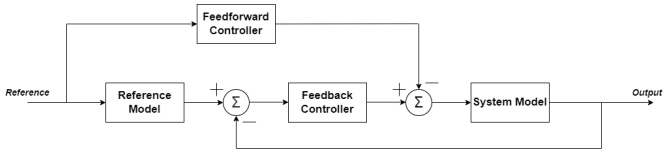

Figure 3.2: *Schematic model of feedforward control for reference tracking.*

to output is then written as

$$\frac{Y(s)}{D(s)} = \frac{1 - F_f(s)G(s)}{1 + F_b(s)G(s)} \tag{3.2}$$

where with perfect control we would get a feedforward controller as

$$F_f(s) = \frac{1}{G(s)}. \tag{3.3}$$

where (3.3) is an ideal feedforward controller removing the impact of the disturbance. Combining a PID controller with a feedforward controller is thus an effective approach to applying an easily implemented controller to tasks where disturbances may affect the system.

There is also the possibility to use feedforward control for improving reference tracking. In a system with a slow reaction time, the time delay between the input and the output can be significant, which can make it difficult to achieve accurate reference tracking using only feedback control. In a system with a slow reaction time, by the time the error is detected and the control inputs adjusted, the output may have already deviated significantly from the desired trajectory. Feedforward control provides the necessary inputs to achieve the desired output trajectory without waiting for feedback from the system. Feedforward control for improved reference tracking uses a model of the reference tracking G_m (how the user wants the reference to be tracked) and a schematic model of feedforward control for reference tracking is shown in Figure 3.2. In terms of a slow-reacting system, the goal of feedforward control for reference tracking is to compensate the feedforward component in regard to the error caused by the slow-responding process.

3.2.2 Model Predictive Control

Model Predictive Control (MPC) is a type of advanced control algorithm that uses a model of a system to make predictions about its future behaviour and then uses those predictions to optimize control inputs to achieve a desired objective. The algorithm repeatedly solves an optimization problem in real-time to compute the control inputs that will drive the system to the desired state, while also taking into account constraints on the system's behaviour [1]. The essence of the prediction of MPC is the receding horizon shown in Figure 3.3.

The receding horizon implies that at time k the algorithm calculates an optimization problem over a predefined prediction horizon p and uses the result to

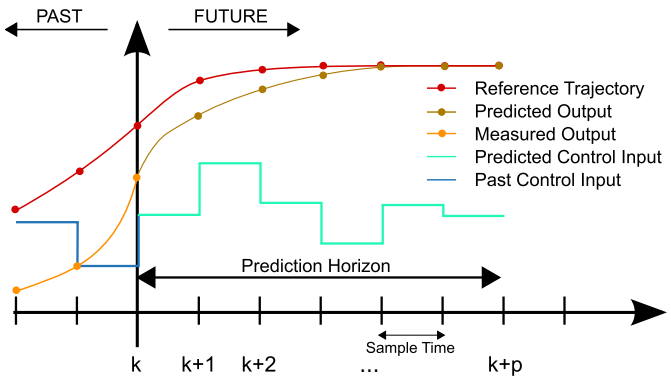

Figure 3.3: *The receding horizon [5].*

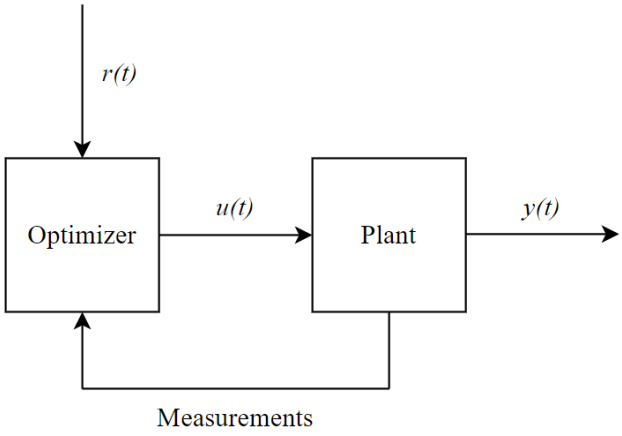

Figure 3.4: *Schematic model of MPC.*

apply an input. At time $k+1$ the same procedure is repeated to calculate the next input [7].

A schematic model of MPC can be viewed in Figure 3.4 where an optimizer calculates the cost function which yields a control input to the plant, or system, in question.

The MPC can therefore be split into three main components: an optimization problem, a model of a system, and constraints on the system's behaviour. The optimization problem is concerned with designing a controller that drives the system state to a reference point while not using an exorbitant control force. The optimization is therefore concerned with optimizing the function of the controller while minimizing the cost of using the function. The process model can be formulated as a state-space model

$$x(k+1) = Ax(k) + Bu(k) \tag{3.4}$$

$$y(k) = Cx(k) \tag{3.5}$$

where $x(k)$ is the state vector, representing the internal state of the process at time k; $u(k)$ is the control input vector; $y(k)$ is the output vector, representing the measurement of the process output at time k. A, B, and C are matrices that describe the relationships between the state, input, and output vectors [11].

The optimization problem is defined as a cost function where the goal is to find the optimal control sequence over a finite time horizon, such that the process satisfies certain constraints and objectives. The optimization problem is formulated as

$$J^*(x_k) \doteq \min_{u_k, u_{k+1} \dots u_{k+N}} \sum_{k=0}^{N} \left(\|x_k\|_{Q_1}^2 + \|u_k\|_{Q_2}^2 \right) \tag{3.6}$$

where $J^*(x_k)$ is the optimal solution to the cost function constrained to the feasible control inputs $\{u_k, u_{k+1} \dots u_{k+N}\}$. x_k are the system variables over a prediction horizon of N and u_k are the input variables: $x_k = x(k+j)$ and $u_k = u(k+j)$ where $j = 0, 1, \dots, N-1$ designating the value of the state and input subject to the prediction horizon N at each time-step j. $\|w_k\|_S^2$ designates the quadratic form $w^T S w$ for $w \in \mathbb{R}^{n_v}$ and $S = S^T \in \mathbb{R}^{n_v \times n_v}$ where S is a weighting matrix - more specifically, in (3.6), Q_1 and Q_2 are weighing matrices specifying the respective cost of states and inputs [20]. The optimization problem is solved at each time step, using the latest measurement information and the predicted state. The first control input in the optimized control sequence is applied to the process, and the process state is updated. The optimization problem is then solved again at the next time step, and so on [15]. One of the primary reasons to apply MPC to a control problem is that the controller, by design, considers system constraints.

The optimization problem can trivially be extended to include reference tracking. By noting the reference signal r one can construct a modified optimization problem

$$J^*(x_k) \doteq \min_{v_k} \sum_{j=0}^{N-1} \left(\|x(k+j) - r(k+j)\|_{Q_1}^2 + \|u(k+j) - u(k+j-1)\|_{Q_2}^2 \right) \tag{3.7}$$

where v_k is the set of all constraints on u. This optimization problem does not weigh the actual input signal u, instead, it considers the input signal's rate of change as a subject to the cost. This is noteworthy as a reference tracking implies $u \neq 0$ to reach the state $x = r$ and as such the value of the input cannot be inherent in the cost [12].

Constrained MPC

Constrained MPC (CMPC) is a type of model predictive control that includes both hard and soft constraints on the system states and inputs. Hard constraints must be satisfied at all times, while soft constraints can be violated for a limited

time or to a limited extent. CMPC is used to design controllers for systems where certain variables or parameters need to be maintained within specific limits or ranges, or where certain physical or operational constraints must be respected [18] [28]. This allows the controller to trade off between tracking the reference trajectory and satisfying the constraints. The optimization problem in CMPC, similar to MPC as shown in Section 3.2.2, involves minimizing a cost function subject to system dynamics, state and input constraints. The solution of the optimization problem provides the optimal control input for the current time step, which is applied to the system. This process is repeated at each time step, allowing the controller to adapt to changing conditions and disturbances while satisfying the constraints. Hard constraints will be modelled as strict inequalities in the optimization problem; as such the hard constraints must be satisfied at each time step. This modelling causes the optimization problem to become infeasible if the constraints are ever violated. The soft constraints will be modelled within the cost function. In this way, a cost will be inscribed for violating the soft constraints, but the model will still function while violating the soft constraints.

4

Method

This chapter presents an evaluation of the control theories, i.e., which control applications are suitable to test empirically. The chapter also features the model equations necessary to construct the MPC controller alongside the implementation of the PID controller and the MPC controller.

4.1 Evaluation of predictive control methods

The core necessary characteristic of the control system is that it must be able to foresee future events: if it is only reacting to current events it will not be able to control the coal boiler without losing power output. Consequently, applying solely a PID controller for the linkage between solar power and coal input will not work. It is for this reason that the PID controller will have to be complemented with a feedforward controller. The reason for using a PID controller and a feedforward controller is simple and needs no academic explanation: the PID controller is the most widely used industrial controller. A PID controller is practically easily implemented, well-known within process control, and is used within a wide range of applications. In this particular case, it is not feasible to use a combination of a PID controller and a feedforward controller. The feedforward controller is incapable of counteracting the slow coal boiler as there are no downstream actuators that can be controlled by it. Even with optimal tuning, the controller will still struggle with time delay. Therefore, attempting to conduct experiments using a PID and conventional feedforward controller would be futile. To achieve practical results, a controller must incorporate predictive features related to solar PV. The PID controller, even with a feedforward term, cannot proactively respond to the incoming solar power. The controller will always react at time $t + 1$, with t being the initial incoming solar power, and its control signal to the boiler will always be responded to at time $t + 1 + \tau$ with τ being

the time constant of the coal boiler. As a result, it cannot react beforehand, even if there is no dynamic present before the coal boiler. This effect is illustrated in Figure 4.1 where at time t_1 the solar power is introduced in the system. The extra effect provided by the solar causes an overshoot of the system until t_2 where the coal boiler is starting to react to the increased effect. This yields an overreaction which peaks at time t_3 before finally being restored at time t_4 where the effect is back to normal. In this scenario, it takes the conventional feedback controller $t_4 - t_1$ seconds to counteract the incoming solar power; the excess power and lack of power will be supplemented by using the battery. Therefore, one goal of the controller is to minimize the time $t_4 - t_1$ and to find an optimum for

$$\min \int_{t_1}^{t_4} \left|\gamma(t)\right| \, dt \tag{4.1}$$

where γ is a model of the usage of the battery.

However, instead of feedforwarding the solar power signal (solar power signal refers to the solar power entering the system) to the controller, it is possible to delay the solar power in relation to the system. This implies using a delay for the solar power signal so that its effects on the system are delayed. By using this approach, one can use a model of how the solar input affects the ratio of the coal input and adjust the coal input ratio in advance of the solar power signal entering the plant.

This approach works as the internal delay of the system is known, see (2.18), and the solar prediction is known. Thus, by applying a delay on the solar power input - a delay in sync with the internal system delay - the system can react in advance to the incoming solar power input and therefore having adjusted the coal input once the delay time has passed; this should result in less volatility in the total power produced by the system. (2.18) also reveals the ratio between coal input ratio to power generation, and therefore how much 1 W of PV produced power should decrease the coal input ratio.

Constrained MPC is a viable choice as it makes a distinction between hard and soft constraints; additionally, it features a predictive element inherent to the controller. Hard constraints are used for parameters such as the steam pressure and the frequency within the complex. The steam pressure and the frequency are variables that have to stay within an acceptable range as too much variability in the variables will cause system damage. Alongside the hard constraints, there are the soft constraints. The soft constraints will be modelled as the efficiency of the system. The efficiency of the system is determined by how well the system uses the power input. There may be cases where there is simply too much energy within the system: i.e., there is an increase in the boiler, the battery is fully charged, and the industrial loads are met, in this case, the system must get rid of the excess energy: in this case, the excess energy can be ousted by opening a valve to release steam. However, as this will waste energy, it is not an optimal solution; yet it is a viable solution and as such it will be modelled as a soft constraint. Another soft constraint is the usage of the battery. In an ideal system, there would be no need for a battery as the solar prediction and its subsequent feedforward

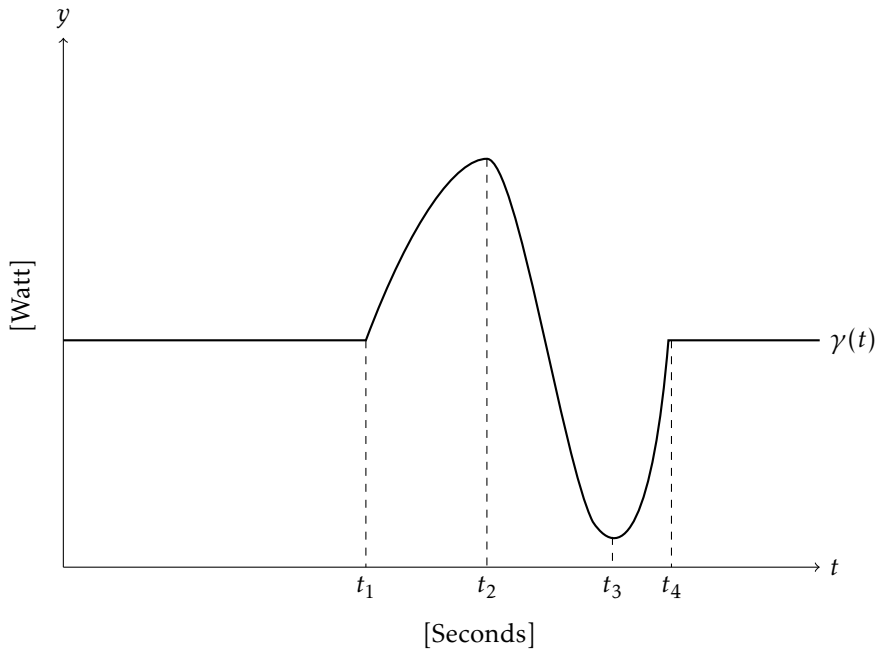

Figure 4.1: *How the power production overshoots.*

control would not require an intermediate storage system: the incoming solar power would signal the boiler to decrease its input and have the system remain in balance. The usage of the battery can therefore be viewed as an evaluation of the performance of the feedforward system - the less the battery is used, the better the feedforward system. But as the battery is a tool, it will be used as such, and as such its usage will be modelled as a soft constraint.

The hard constraints are modelled by

$$x_l \leq x(n) \leq x_u \;\&\; u_l \leq u(n) \leq u_u, \text{ for } n = 0, \ldots, N-1 \tag{4.2}$$

where $x(n) \in \mathbb{R}^{n_h}$ are the system states and $u(n) \in \mathbb{R}^{n_h}$ the system inputs for the number of hard constraints, n_h, at each time step n subject to the lower and upper constraints x_l and x_u for the system states and u_l and u_u for the system inputs.

Similarly, the soft constraints are modelled by

$$x_l \leq x(n) \leq x_u \;\&\; u_l \leq u(n) \leq u_u, \text{ for } n = 0, \ldots, N-1 \tag{4.3}$$

where $x(n) \in \mathbb{R}^{n_s}$ are the system states and $u(n) \in \mathbb{R}^{n_s}$ the system inputs for the number of soft constraints, n_s, at each time-step n subject to the lower and upper constraints x_l and x_u for the system states and u_l and u_u for the system inputs. The values on hard and soft constraints are presented in Section 4.3.

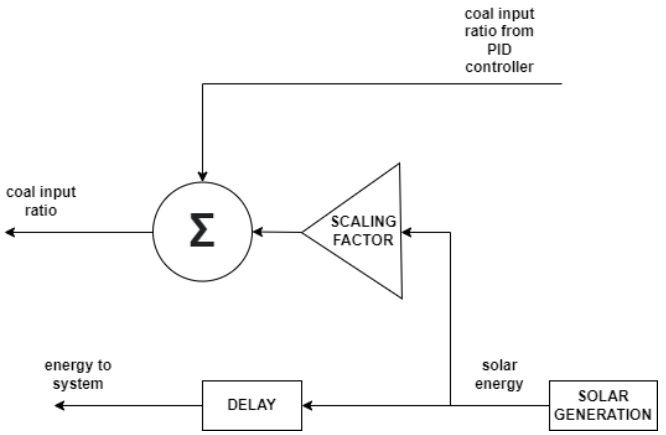

Figure 4.2: *Schematic figure of the introduced delay.*

4.2 Simulation setup

To evaluate the PID and feedforward approach, a delay block will be entered into the Dymola model to make the solar power enter the system at a delayed time while the solar power that influences the coal input ratio enters immediately; this approach is shown in Figure 4.2 where the amount of coal being inserted into the boiler will be modified in advance of the actual solar power entering the system. The scaling factor has been verified empirically by studying how the coal input ratio affects steam production and therefore how much increased power production should decrease the coal input ratio to $2.98 \cdot 10^{-9}$.

The implementation of the MPC controller uses both Dymola and MATLAB. The simulation setup works as the following: The Dymola model has the plant model for the industrial complex (subject to simplifications) and will be exported to Simulink by using an FMU block. The MPC controller will use the equality constraints from the Dymola model as the plant in the MPC controller. Therefore, the MPC controller will be generated as the plant over the prediction horizon. This is constructed in the format

$$Ax = b \tag{4.4}$$

where x serves as the system states, where $A \in \mathbb{R}^{(4p+4+13)\times(6p+6)}$, $x \in \mathbb{R}^{(6p+6)\times 1}$, and $b \in \mathbb{R}^{(4p+4+13)\times 1}$. The dimensions are based on the number of physical constraints and the prediction horizon. The 4 system states are the generated frequency, the battery's state of charge, the steam power production, and the total power production throughout the prediction horizon. The 2 control signals are the battery state energy charging and the coal input ratio; the 2 control signals are modelled as system states but serve as control signals by their implementation. The 4 system states are fully modelled within the $Ax = b$ model; the $Ax = b$ model will serve to generate the physical constraints, through equality constraints, of the system. The optimizer is therefore not free to choose these values: they are set by the

equality constraints. The coal input ratio will have its first 13 inputs modelled within the $Ax = b$ model as these values are bounded by the previous iterations coal input ratios. This is due to the inherent delay in the steam generator making the first 13 coal input ratios determined by the previous iteration's control inputs. The rest of the control signals are free to choose by the optimizer unbounded by equality constraints.

The $Ax = b$ model will have each state in each time step up to the prediction horizon. This is so that the MPC can review all states up until the prediction horizon to find the optimum control sequence. The state vector x is therefore written

$$x = \begin{bmatrix} x_{f,1} \\ \vdots \\ x_{f,p+1} \\ x_{SOC,1} \\ \vdots \\ x_{SOC,p+1} \\ x_{P_s,1} \\ \vdots \\ x_{P_s,p+1} \\ x_{P_{tot},1} \\ \vdots \\ x_{P_{tot},p+1} \\ x_{c,1} \\ \vdots \\ x_{c,p+1} \\ x_{B,1} \\ \vdots \\ x_{B,p+1} \end{bmatrix}$$

The matrices A and b are (2.5) (2.16) (2.23) (2.26), with the additional 13 first coal ratio control inputs. Let A_f represent the part of the A matrix building up the generated frequency equation, A_{SOC} for the SOC, etc. Below are the matrices that build up $Ax = b$. The equality constraints for the frequency are given by

$$A_f x = b_f \tag{4.5}$$

and can be viewed in the equation below where $A_f \in \mathbb{R}^{(p+1)\times(6p+6)}$, $x \in \mathbb{R}^{(6p+6)\times 1}$, and $b_f \in \mathbb{R}^{(p+1)\times 1}$. $K_1 = \frac{K_{lin} \cdot t_s}{(2\pi)^2}$, $S = 2.44 \cdot 10^8$ which scales the states, and $K_2 = \frac{K_{lin} \cdot t_s}{(2\pi)^2}$ which likewise scales the battery charging to correct dimension. The initial frequency $x_{f,init}$ is set to 0 Hz (50 Hz non-linearized).

$$\begin{pmatrix} -1 & 0 & \cdots & 0 & 0 & 0 & 0 \cdots & 0 & 0 & 0 & 0 \cdots & 0 & 0 \\ 1 & -1 & \cdots & 0 & 0 & K_1 S & 0 \cdots & 0 & 0 & K_1 S & 0 \cdots & 0 & 0 \\ \vdots & & & & & & & & & & & & \\ 0 & 0 & \cdots & -1 & 0 & 0 & 0 \cdots & 0 & 0 & 0 & 0 \cdots & 0 & 0 \\ 0 & 0 & \cdots & 1 & -1 & 0 & 0 \cdots & 100K_2 & 0 & 0 & 0 \cdots & 100K_2 & 0 \end{pmatrix} \cdot \begin{pmatrix} x_{f,1} \\ x_{f,2} \\ \vdots \\ x_{f,p} \\ x_{f,p+1} \\ x_{P_{tot},1} \\ x_{P_{tot},2} \\ \vdots \\ x_{P_{tot},p} \\ x_{P_{tot},p+1} \\ x_{B,1} \\ x_{B,2} \\ \vdots \\ x_{B,p} \\ x_{B,p+1} \end{pmatrix} = \begin{pmatrix} x_{f,init} \\ K_2 P_{load} \\ \vdots \\ K_2 P_{load} \\ K_2 P_{load} \end{pmatrix}$$

The equality constraints for the SOC are given by

$$A_{SOC} x = b_{SOC} \tag{4.6}$$

with scaling factors where $A_{soc} \in \mathbb{R}^{(p+1)\times(6p+6)}$, $x \in \mathbb{R}^{(6p+6)\times 1}$, and $b_{soc} \in \mathbb{R}^{(p+1)\times 1}$ which can be viewed in the equation below. The initial SOC $x_{SOC,init}$ is set to 0.5 to set the initial SOC to 50% of maximum capacity.

$$\begin{pmatrix} \cdots -1 & 0 & \cdots & 0 & 0 & \cdots & 0 & 0 \cdots & 0 & 0 \\ \cdots 1 & -1 & \cdots & 0 & 0 & \cdots & \frac{100 t_s}{10^{11}} & 0 \cdots & 0 & 0 \\ \vdots & & & & & & & & & \\ \cdots 0 & 0 & \cdots & -1 & 0 & \cdots & 0 & 0 \cdots & 0 & 0 \\ \cdots 0 & 0 & \cdots & 1 & -1 & \cdots & 0 & 0 \cdots & \frac{100 t_s}{10^{11}} & 0 \end{pmatrix} \cdot \begin{pmatrix} \vdots \\ x_{SOC,1} \\ x_{SOC,2} \\ \vdots \\ x_{SOC,p} \\ x_{SOC,p+1} \\ \vdots \\ x_{B,1} \\ x_{B,2} \\ \vdots \\ x_{B,p} \\ x_{B,p+1} \end{pmatrix} = \begin{pmatrix} -x_{SOC,init} \\ 0 \\ \vdots \\ 0 \\ 0 \end{pmatrix}$$

The equality constraints for steam power generation are given by

$$A_{steam} x = b_{steam} \tag{4.7}$$

with scaling factors. $K_1 = 1.255 \cdot 10^7$ and $K_2 = 0.9626$ which comes from (2.23). $S = 2.44 \cdot 10^8$ which scales the states where $A_{steam} \in \mathbb{R}^{(p+1)\times(6p+6)}$, $x \in \mathbb{R}^{(6p+6)\times 1}$,

and $b_{steam} \in \mathbb{R}^{(p+1)\times 1}$, which can be viewed below. The initial steam power generation $x_{p,init}$ is set to 1 which is the energy production needed to counteract the plant's internal load.

$$\begin{pmatrix} \cdots -1 & 0 & \cdots & 0 & 0 & \cdots & 0 & 0 & \cdots & 0 & 0 & \cdots \\ \cdots K_1 S & -S & \cdots & 0 & 0 & \cdots & K_2 & 0 & \cdots & 0 & 0 & \cdots \\ \vdots & & & & & & & & & & & \\ \cdots 0 & 0 & \cdots & -S & 0 & \cdots & 0 & 0 & \cdots & 0 & 0 & \cdots \\ \cdots 0 & 0 & \cdots & K_1 S & -S & \cdots & 0 & 0 & \cdots & K_2 & 0 & \cdots \end{pmatrix} \cdot \begin{pmatrix} \vdots \\ x_{P_s,1} \\ x_{P_s,2} \\ \vdots \\ x_{P_s,p} \\ x_{P_s,p+1} \\ \vdots \\ x_{c,1} \\ x_{c,2} \\ \vdots \\ x_{c,p} \\ x_{c,p+1} \end{pmatrix} = \begin{pmatrix} -x_{P_s,init} \\ 0 \\ \vdots \\ 0 \\ 0 \end{pmatrix}$$

The equality constraints for the total power generation are given by

$$A_{tot} x = b_{tot} \tag{4.8}$$

with scaling factors. $K_1 = 1.255 \cdot 10^7$ and $K_2 = 0.9626$ which comes from (2.23). $S = 2.44 \cdot 10^8$ which scales the states where $A_{tot} \in \mathbb{R}^{(p+1)\times(6p+6)}$, $x \in \mathbb{R}^{(6p+6)\times 1}$, and $b_{tot} \in \mathbb{R}^{(p+1)\times 1}$. One can note that it is inside the b-matrix that solar power enters the system. The equality constraints are shown below. The initial total power generation $x_{P_{tot},init}$ is set to 1 which is the energy production needed to counteract the plant's internal load.

$$\begin{pmatrix} \cdots & 0 & 0 \cdots & 0 & 0 \cdots -1 & 0 & \cdots & 0 & 0 & \cdots & 0 & 0 \cdots & 0 & 0 \\ \cdots K_1 S & 0 \cdots & 0 & 0 \cdots & 0 & -S \cdots & 0 & 0 & \cdots K_2 & 0 \cdots & 0 & 0 \\ \vdots & & & & & & & & & & & & & \\ \cdots & 0 & 0 \cdots & 0 & 0 \cdots & 0 & 0 & \cdots -S & 0 & \cdots & 0 & 0 \cdots & 0 & 0 \\ \cdots & 0 & 0 \cdots K_1 S & 0 \cdots & 0 & 0 & \cdots & 0 & -S \cdots & 0 & 0 \cdots K_2 & 0 & & \end{pmatrix} \cdot \begin{pmatrix} \vdots \\ x_{P_s,1} \\ x_{P_s,2} \\ \vdots \\ x_{P_s,p} \\ x_{P_s,p+1} \\ \vdots \\ x_{P_{tot},1} \\ x_{P_{tot},2} \\ \vdots \\ x_{P_{tot},p} \\ x_{P_{tot},p+1} \\ \vdots \\ x_{c,1} \\ x_{c,2} \\ \vdots \\ x_{c,p} \\ x_{c,p+1} \end{pmatrix} = \begin{pmatrix} -x_{P_{tot},init} \\ -P_{sol,1} \\ \vdots \\ -P_{sol,p-1} \\ -P_{sol,p} \end{pmatrix}$$

The equality constraints for the coal input ratio are given by

$$A_{coal} x = b_{coal} \tag{4.9}$$

where $A_{coal} \in \mathbb{R}^{13 \times (6p+6)}$, $x \in \mathbb{R}^{(6p+6) \times 1}$, and $b_{coal} \in \mathbb{R}^{13 \times 1}$. It is here that the control delay enters the system. The 13 first control inputs are bounded by the 13 control inputs from the previous optimization iteration which are noted in the b-matrix (the delay control inputs). The remaining control inputs feature no equality constraints and are therefore chosen by the optimizer. The equality constraints are shown below.

$$\begin{pmatrix} \cdots & 1 & 0 & 0 & \cdots & 0 & \cdots \\ \cdots & 0 & 1 & 0 & \cdots & 0 & \cdots \\ \cdots & 0 & 0 & 1 & \cdots & 0 & \cdots \\ \vdots & & & & & & \\ \cdots & 0 & 0 & 0 & \cdots & 1 & \cdots \end{pmatrix} \cdot \begin{pmatrix} \vdots \\ x_{c,1} \\ x_{c,2} \\ x_{c,3} \\ \vdots \\ x_{c,13} \\ \vdots \end{pmatrix} = \begin{pmatrix} x_{c_d,1} \\ x_{c_d,2} \\ x_{c_d,3} \\ \vdots \\ x_{c_d,13} \end{pmatrix}$$

4.3 CMPC implementation

The hard constraints on the system states of the MPC (the normed constraints) can be viewed in Table 4.1 and the hard constraints for the PID are shown in

Table 4.1: *Hard constraints on system states for the MPC.*

State	Lower limit	Upper limit	Unit
System frequency	-0.5	0.5	Hz
SOC	0	1	-
Steam power production	0.595	1.635	-
Total power production	0.595	N/A	-
Coal ratio	0.5	1.3	-
Battery charging	$\zeta(x_{soc})$	$\zeta(x_{soc})$	-

Table 4.2: *Hard constraints on system states for the PID.*

State	Lower limit	Upper limit	Unit
System frequency	49.5	50.5	Hz
SOC	0	28	MWh
Steam power production	$1.452 \cdot 10^8$	$3.989 \cdot 10^8$	Watt
Total power production	$1.452 \cdot 10^8$	N/A	Watt
Coal ratio	0.5	1.3	-
Battery charging	$\zeta(x_{soc})$	$\zeta(x_{soc})$	Watt

Table 4.2. The tables show each state's lower and upper limits. The system frequency is bound between -0.5 and 0.5 which, non-linearized, is between 49.5 and 50.5 Hz which is the acceptable industry standard. The steam power generation's lower limit is the cap at which the steam inside the system turns into water, and its upper limit is the limit at which the built-up steam inside the system is capped: higher power production produces a steam pressure that needs to be released and as such decreases the energy efficiency of the system. All system states are modelled to be around the value of 1, this is due to the optimizer performing better when the system states are not in various orders of magnitude. As such, the battery SOC is modelled to be between 0 and 1 which implies a scaling factor of 10^{11}. The coal ratio is bound between 0.5 and 1.3 as this is the limit for the system to handle rapid changes in generated steam power. The total power generation has no inherent maximum value as the other constraints are dependent on the total power generation. The steam and total power production are scaled by $2.44 \cdot 10^8$ to make the steam power production of 1 equal to the internal plant load: all values above 1 imply that the steam power production is larger than the internal plant load and that the excess power will enter the battery; all values below 1 imply that the battery has to de-charge to cover for the insufficient power generation.

The full CMPC model is constructed by stacking the five A_i and b_i matrices to construct a complete $Ax = b$ model and by inserting the constraints into the optimizer. The CMPC model is built in MATLAB using the $fmincon$ function to generate the optimizer. $fmincon$ is a gradient-based optimization method which

works by finding the minimum of a problem as specified by

$$\min_x f(x) \text{ subject to } \begin{cases} c(x) \leq 0 \\ ceq(x) = 0 \\ A \cdot x \leq b \\ Aeq \cdot x = beq \\ lb \leq x \leq ub \end{cases} \tag{4.10}$$

where the problem specification serves as the physical properties and the operating constraints within the system [23]. The optimizer's objective function is to minimize the difference between the SOC and the reference value of 0.5 - the state at which the battery is 50% charged; minimize the range of the frequency; minimize the rate of change for the coal input ratio; and finally to minimize the difference between the total power generation and the load; i.e., the optimizer should look over the entire prediction horizon and choose the control inputs that best minimize

$$f(x) = \sum_{i=1}^{p+1} \left(Q_1 \cdot (x_{SOC,i} - 0.5)^2 + Q_2 \cdot x_{f,i}^2 + Q_3 \cdot (\Delta x_c)^2 + Q_4 \cdot (x_{P_{tot,i}} - 1)^2 \right). \tag{4.11}$$

The scalars Q_1, Q_2, Q_3, and Q_4 are weighing scalars reflecting on the importance of minimizing each variable. The objective function can be viewed as the soft constraints on the system: the optimizer will steer to achieve the objective function but will prioritize the hard constraints in its operation. The optimization problem is implemented in MATLAB. The optimization problem updates over the scenario time by inserting the optimal values at time t into the initial values of the optimizer at time $t + 1$. The upper and lower bounds, ub and lb are set to the constraints noted in Table 4.1. The initial guess $x0$ of the optimizer is set to 0 for all states. The control input is updated by taking the 14th time step of the control sequence, and placing it last in the control sequence as the following:

$$\begin{aligned} t = 1: &\quad x_{c_d} = (x_{c,1}, x_{c,2}, \ldots, x_{c,13}) \\ t = 2: &\quad x_{c_d} = (x_{c,2}, x_{c,3}, \ldots, x_{c,14}) \\ &\vdots \\ t = 13: &\quad x_{c_d} = (x_{c,13}, x_{c,14}, \ldots, x_{c,25}) \end{aligned}$$

which updates the $A_{coal}x = b_{coal}$ system, where x_{c_d} is the state of the control delay.

The $Ax = b$ model is generated into a "MATLAB Function" block in Simulink where its inputs are the outputs of the Dymola FMU Plant block and its outputs are the inputs to the Dymola FMU plant block. This way, the MPC will from its inherent $Ax = b$ model, which is the plant-modelled simplified, yield the plant's optimal inputs and then change the outputs accordingly to the plant's outputs.

5
Results

In this section, the results from applying the PID controller with the delay modification and the MPC controller are presented.

5.1 Feedforward-based predictive controller

For the following figures, the red line is the results from the delay-modified model, and the blue line is the baseline model. Two tests will be performed for the PID controllers: one where the solar power enters as a ramp signal, and one where the solar power enters as a step signal. This is to test the robustness of the control system in terms of solar power intensity. The solar power entering the system is set to 40% of the total power requirement of the plant and enters the system at 15000 seconds. The solar signal enters as a ramp signal with a duration of 2000 seconds and leaves the system at 20000 seconds as a ramp signal of 2000 seconds. The step solar power enters the system at 15000 seconds and leaves at 20000 seconds. The scaling factor of the delayed signal is set to $2.98 \cdot 10^{-9}$, see Section 4.2, and the delay time is set to 200 seconds to account for the inherent system dynamics. Note that the variables are not normed for the PID controller as for the MPC controller, therefore the constraints are based on Table 4.2.

Applying the delay-modified PID controller onto the system obtains the following results. The usage of the battery decreases, as shown in Figures 5.1 and 5.2. For the ramp solar experiment, the battery SOC volatility decreases from a range of $SOC_{vol} \in [-31.1\%, +32.3\%]$ to $SOC_{vol} \in [-5.61\%, +4.81\%]$ implying that a smaller battery is required when applying the delay-modification to the plant. For the step signal solar experiment, the battery SOC volatility decreases from a range of $SOC_{vol} \in [-69.4\%, +67.2\%]$ to $SOC_{vol} \in [-19.8\%, +20.0\%]$. The need for the battery decreases as the volatility of the total power production decreases as further shown in Figures 5.3 and 5.4. The total power volatility de-

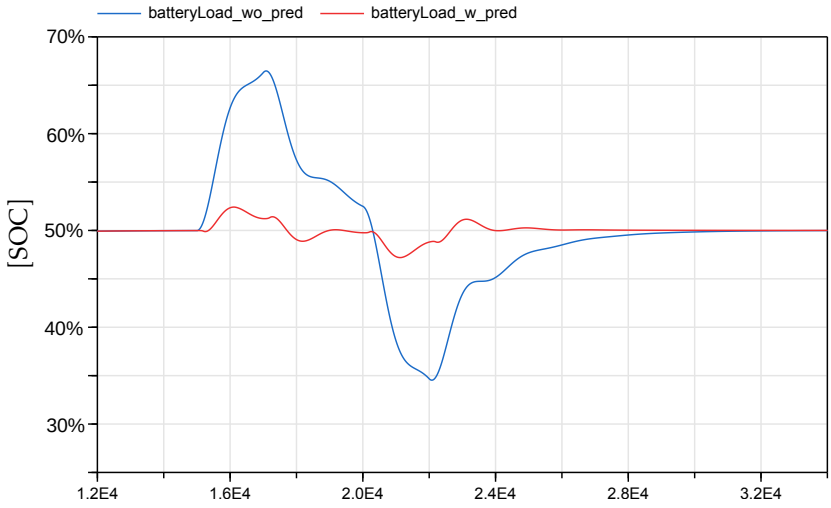

Figure 5.1: *PID controller - SOC for ramp solar signal.*

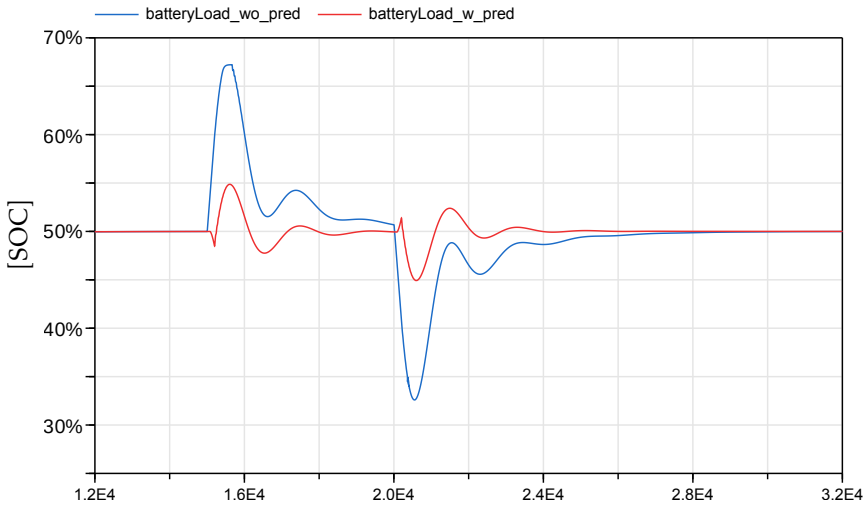

Figure 5.2: *PID controller - SOC for step solar signal.*

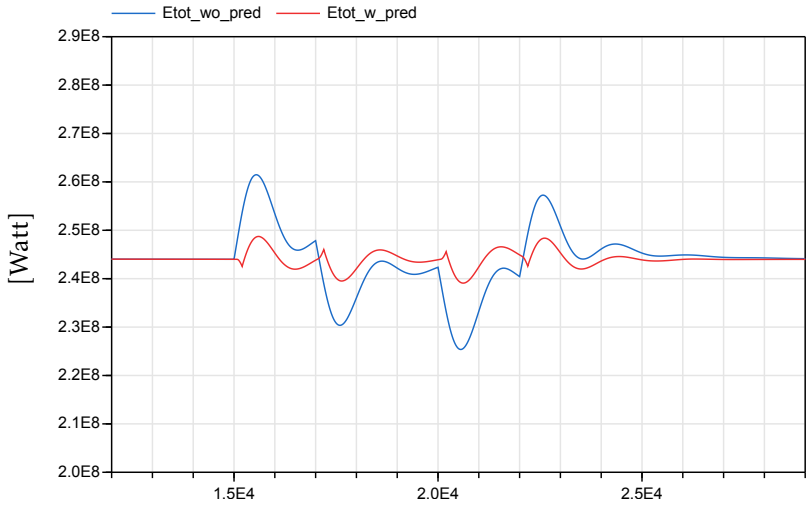

Figure 5.3: *PID controller - total power production volatility for ramp solar signal.*

creased from $P_{tot,vol} \in [-7.62\%, +7.17\%]$ to $P_{tot,vol} \in [-2.01\%, +1.93\%]$ for the ramp solar experiment and the total power volatility decreased from $P_{tot,vol} \in [-41.8\%, +41.4\%]$ to $P_{tot,vol} \in [-35.7\%, +25.0\%]$ for the step signal experiment which yields the plant a steadier power flow. The introduction of the delay modification has therefore caused the power output to become more constant in comparison to the baseline model. The coal input has likewise become more responsive to the incoming solar power. The coal input reacts accordingly to the introduced delay to decrease the amount of coal entering the system before the solar power enters the system as shown in Figures 5.5 and 5.6. The delay-modified model decreases the coal input before the non-modified model and therefore does not have to decrease the amount of coal input as much as the non-modified model. Per stability, Figure 5.8 reveals the frequency of both systems which shows that for the step solar experiment, neither controller is within acceptable bounds. Figure 5.7 shows that both models are stable for the solar ramp signal. The steam pressure is stable for all tested systems as the steam release controller releases no steam and as such the system is running under maximum energy efficiency.

5.2 MPC

The solar prediction is considered ideal - the prediction model has a complete overview of the incoming solar power. Two tests will be performed: one where the solar enters as a step signal, and one where the solar power enters and leaves as a ramp signal, where the ramp is of length 250 seconds (25 samples in terms

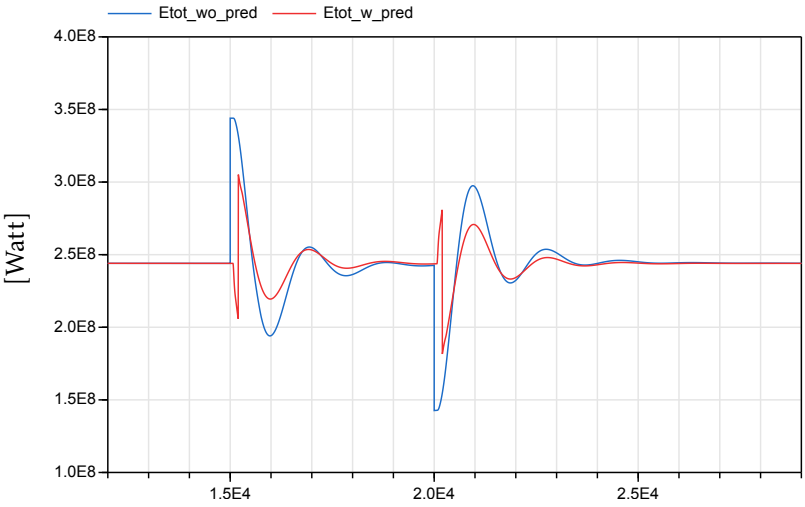

Figure 5.4: *PID controller - total power production volatility for step solar signal.*

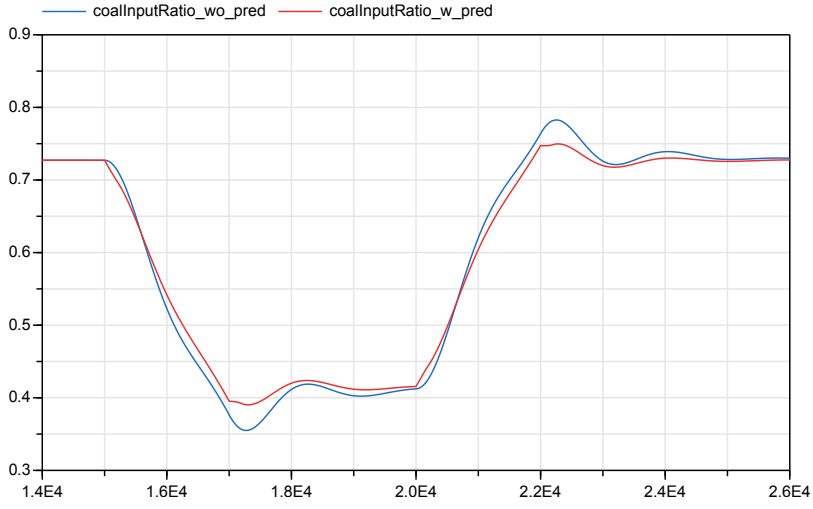

Figure 5.5: *PID controller - coal input ratio for ramp solar signal.*

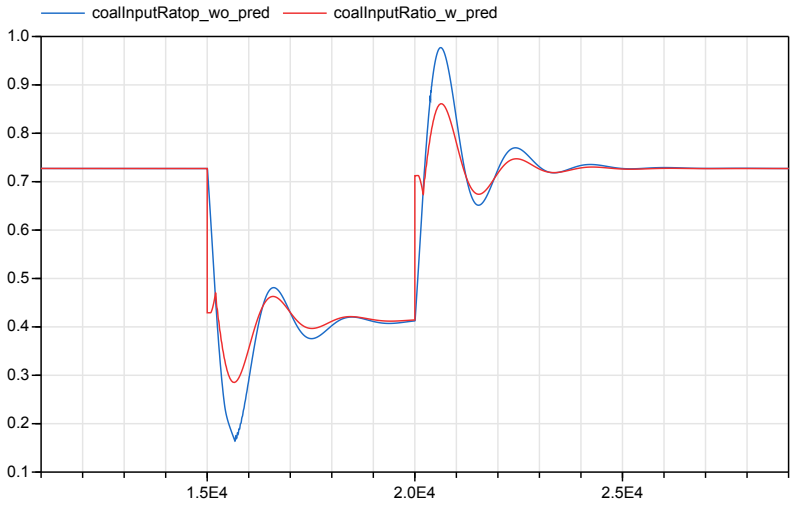

Figure 5.6: *PID controller - coal input ratio for step solar signal.*

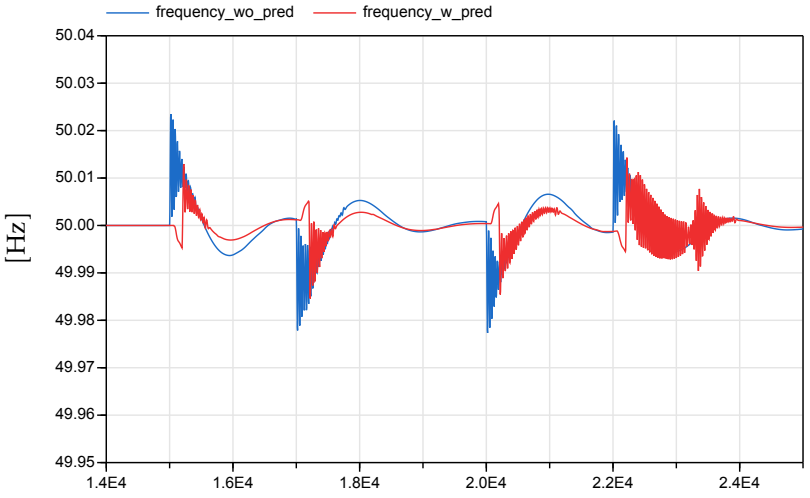

Figure 5.7: *PID controller - frequency generation for ramp solar signal.*

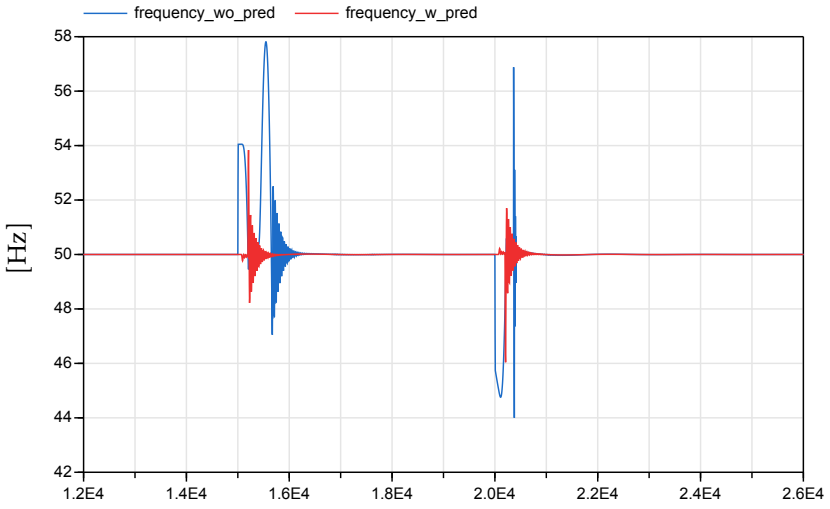

Figure 5.8: *PID controller - frequency generation for step solar signal.*

of the sampling rate). The incoming solar power enters the system at the time

$$0.25 \cdot T_s = 1250 \tag{5.1}$$

and leaves the system at

$$0.5 \cdot T_s = 2500 \tag{5.2}$$

for the step test, and at

$$0.2 \cdot T_s = 1000 \tag{5.3}$$

and leaves the system at

$$0.55 \cdot T_s = 2750 \tag{5.4}$$

for the ramp test, where T_s is the scenario's simulation time - T_s will be set to 5000 seconds for MPC controller experiments. The two tests are designed to evaluate the controllers' performance to various difficulties in incoming solar power. Both the prediction horizon and control horizon are set to 60. This gives the optimizer a horizon of 600 seconds, considering the sampling rate, to evaluate the incoming solar power. The weighing scalars in the optimization problem (4.11) are set to

$$\begin{aligned} Q_1 &= 1 \\ Q_2 &= 5 \cdot 10^{-4} \\ Q_3 &= 0.25 \\ Q_4 &= 1 \end{aligned}$$

which were found empirically.

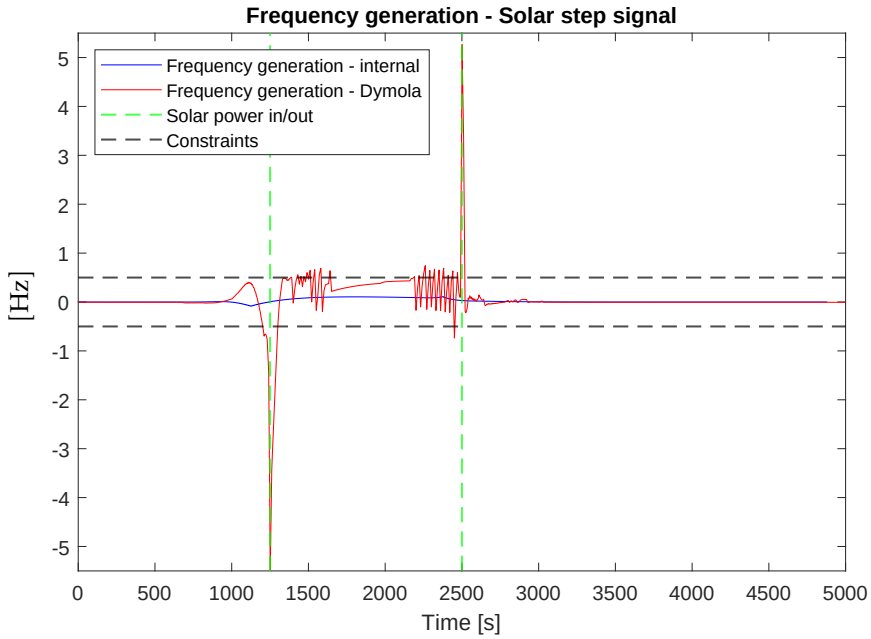

Figure 5.9: *Frequency generation of both models. 0 Hz is the normed linearization representative of 50 Hz.*

Solar power step signal

Figure 5.9 shows the frequency generation when the solar enters as a step signal for the MPC modelled running on itself and the MPC model runs on the Dymola model. When running on its own model, the controller successfully controls the frequency within its acceptable bounds; however, for the Dymola model, this is not the case as the frequency becomes unstable once the solar power enters the system. Figure 5.10 shows the state of charge for the MPC running on its internal model and the MPC model running on the Dymola model. Both models have their battery SOC stable throughout the simulation time and there is hardly a difference in the SOC of the models throughout the simulation time. The MPC controller running on its internal model yields a state of charge volatility in the range $SOC_{vol} \in [-6.66\%, +8.56\%]$ and the MPC model running on the Dymola model yields the range $SOC_{vol} \in [-6.04\%, +9.74\%]$. Figure 5.11 shows the steam power generation for the MPC model running on its internal model and the MPC-Dymola model over the scenario time. The steam power generation is similar for both models with slight volatility observed in the Dymola model. Figure 5.12 shows the total power generation over the scenario time for the MPC internal model and the MPC-Dymola model. As a consequence of the steam power generation, the total power generation will be slightly volatile for the Dymola model. This is natural as it is a direct function of the generated steam power. Running the MPC controller on its internal model produces a total power volatility of

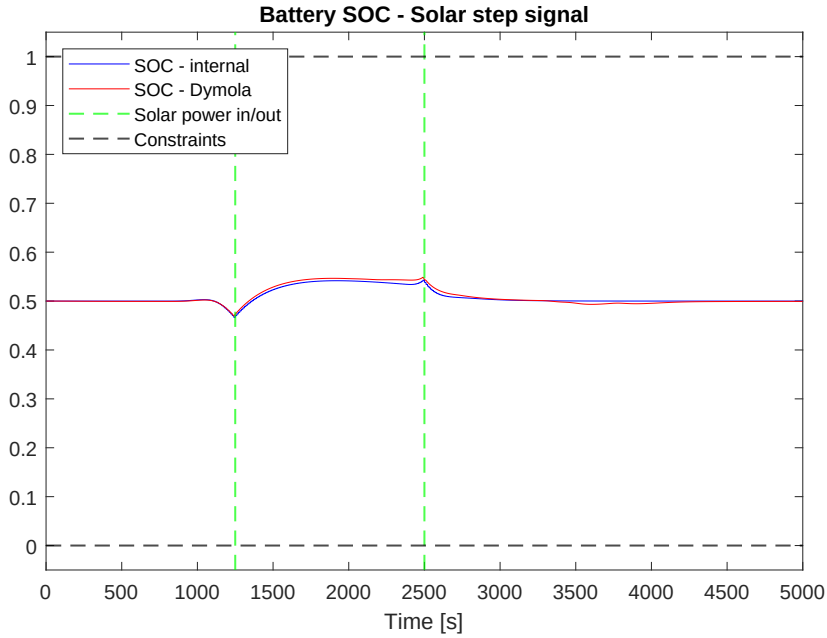

Figure 5.10: *SOC of both models.*

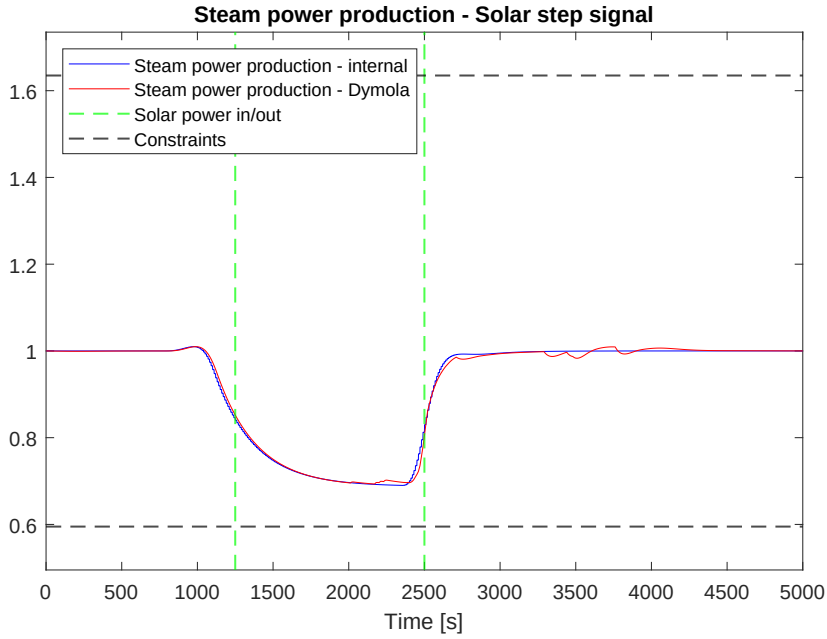

Figure 5.11: *Steam power generation of both models.*

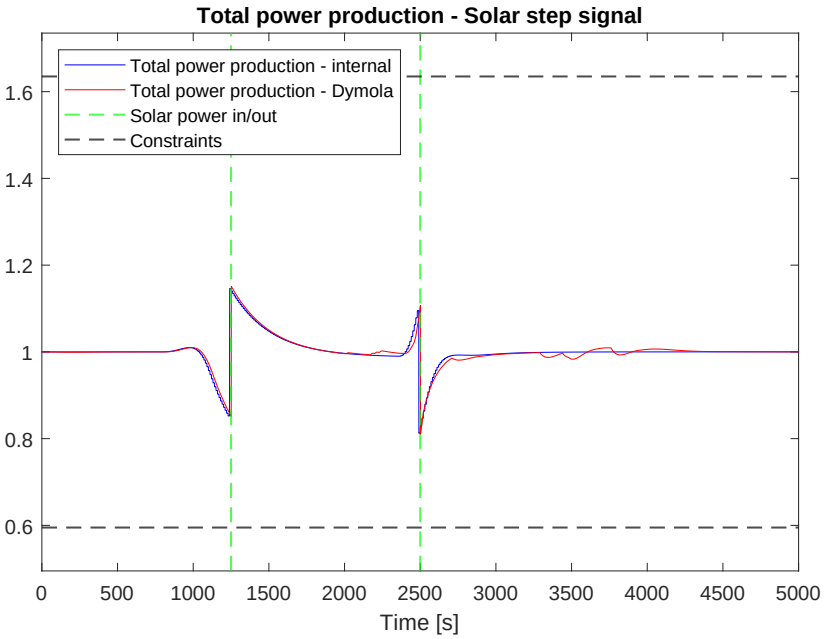

Figure 5.12: *Total power generation of both models.*

$P_{tot,vol} \in [-18.75\%, +14.61\%]$ and running on the Dymola model yields a range $P_{tot,vol} \in [-19.02\%, +15.09\%]$. Figure 5.13shows the coal input ratio for both models throughout the simulation. The coal input ratio reacts accordingly to the incoming solar power, with a greater, yet slower, reaction by the Dymola model. They both adjust the coal input ratio before the solar power enters the system and before the solar power leaves the system. The coal input ratio for the Dymola model reveals the volatility in both the generated steam power and in the total generated power: volatility in the coal input ratio ripples into the generated steam power.

Solar power ramp signal

Figure 5.14 shows the frequency generation when the solar enters as a ramp signal for the MPC modelled running on itself as well as the MPC model running on the Dymola model. Noteworthy is that the frequency is within the constraints when the MPC is running on its own internal model; however, the frequency becomes unstable once the MPC runs on the Dymola model. Figure 5.15 shows the state of charge for the battery over the scenario time. For both the MPC's internal model and the Dymola model, the battery's SOC is within acceptable bounds throughout the simulation period and there is very little difference in its value for both scenarios. The MPC controller, running on its own internal model, yields a battery load volatility of $SOC_{vol} \in [-2.80\%, +7.14\%]$ and while running on the Dymola model, yields a battery load volatility of $SOC_{vol} \in [-2.23\%, +8.12\%]$. Fig-

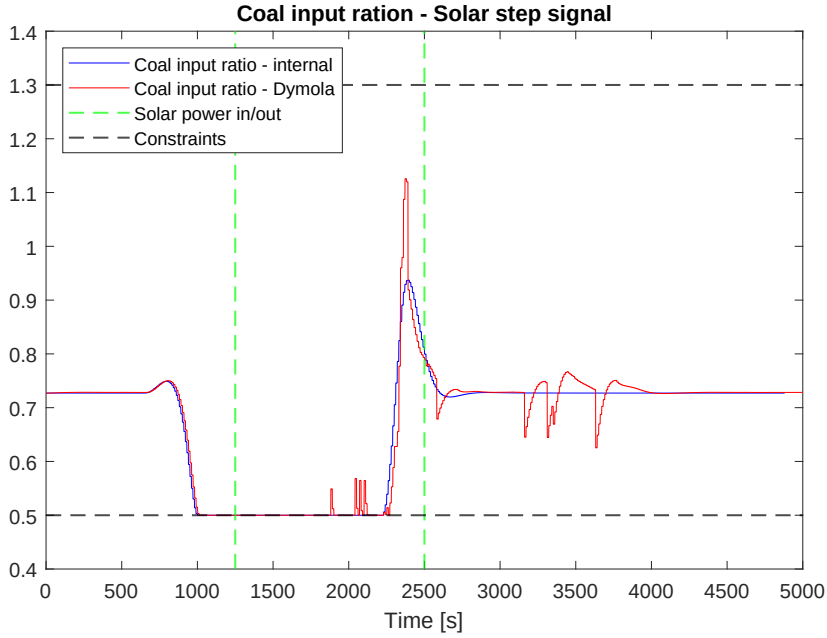

Figure 5.13: *Coal input ratio of both models.*

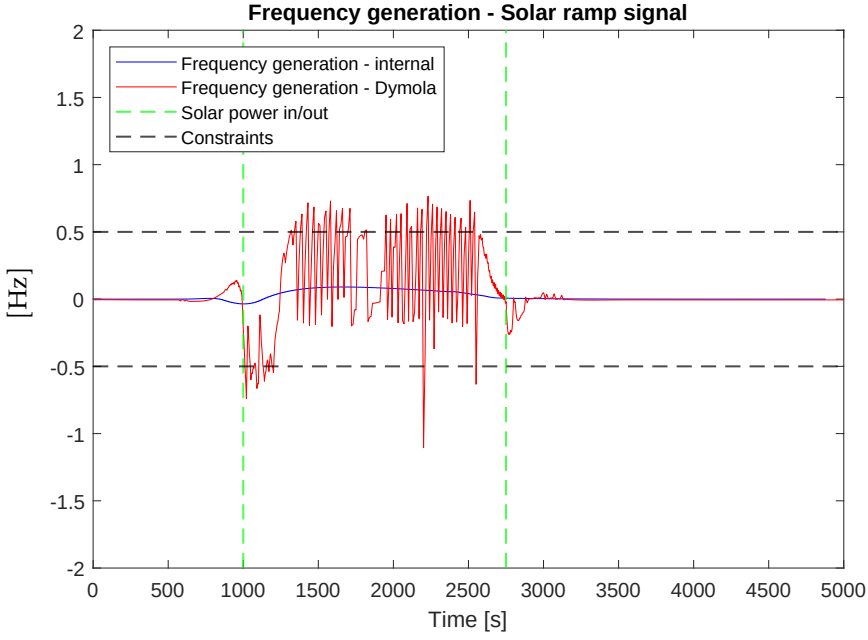

Figure 5.14: *Frequency generation of both models. 0 Hz is the normed linearization representative of 50 Hz.*

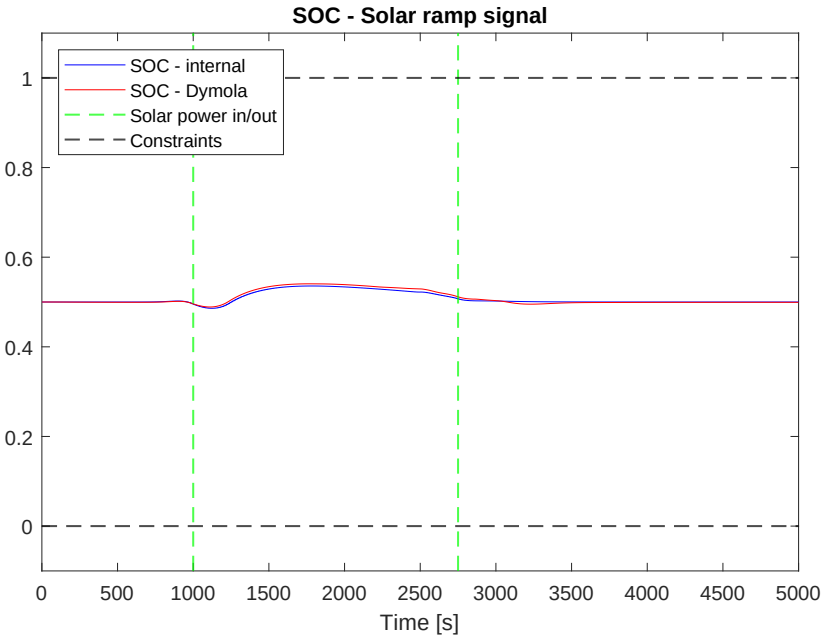

Figure 5.15: *SOC of both models.*

ure 5.16 shows the steam power production for both models. The steam power production is similar for both models; the sole difference being slight volatility in the Dymola model's steam power production. Figure 5.17 shows the total power production for both models. As a consequence of the steam power production volatility, the total power production will naturally be slightly volatile for the Dymola model. The total power production fluctuates slightly from the set-point of 1. The MPC running on its internal model yields a total power volatility of $P_{tot,vol} \in [-5.89\%, +8.54\%]$ and for the Dymola model a total power volatility of $P_{tot,vol} \in [-5.93\%, +8.79\%]$. Figure 5.18 shows the coal input ratio for both models. Both models' coal input ratios react accordingly to the incoming solar power. They adjust the coal input ratio before the solar power enters the system and before the solar power leaves the system. The figure reveals the reasoning for the volatility of the Dymola model's steam power production: the coal input ratio features a few rapid increases and as such causes the produced steam power to spike in production at certain time spots.

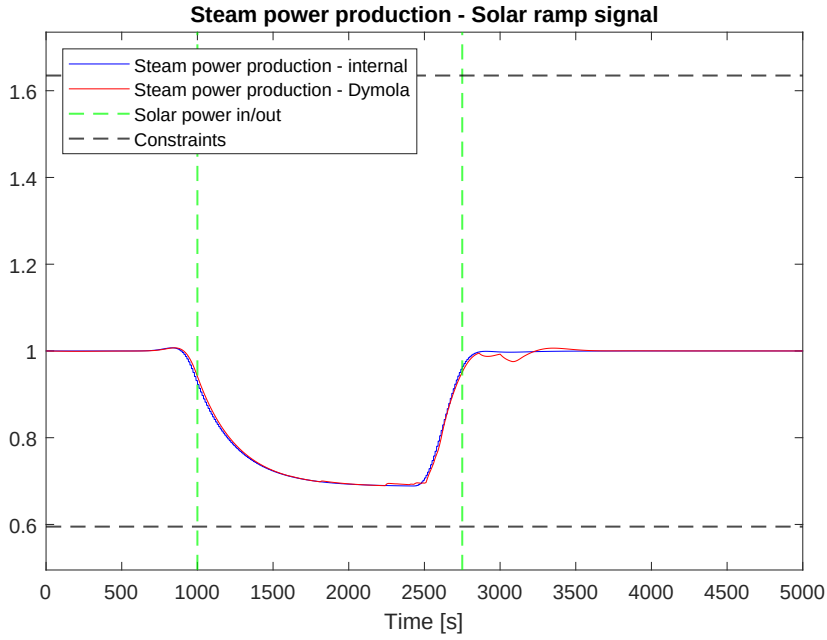

Figure 5.16: *Steam power generation of both models.*

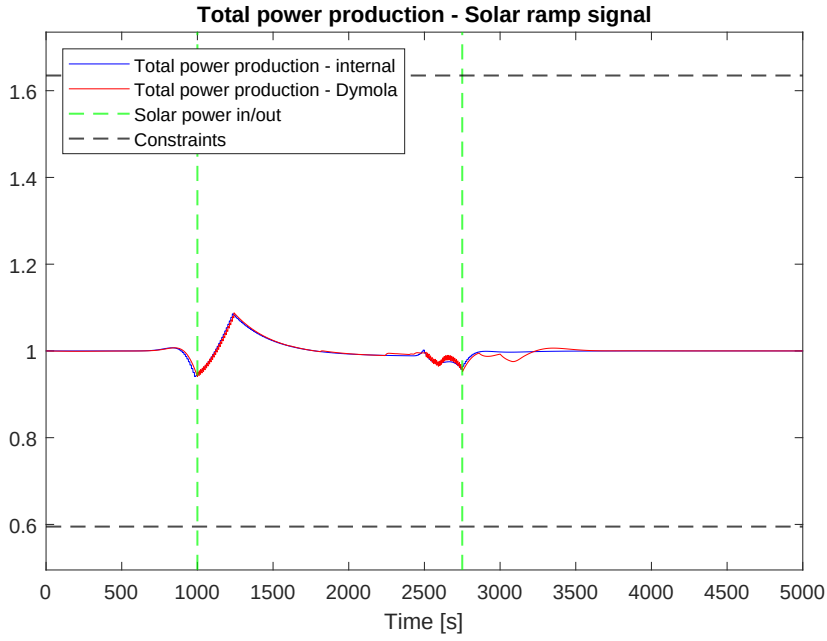

Figure 5.17: *Total power generation of both models.*

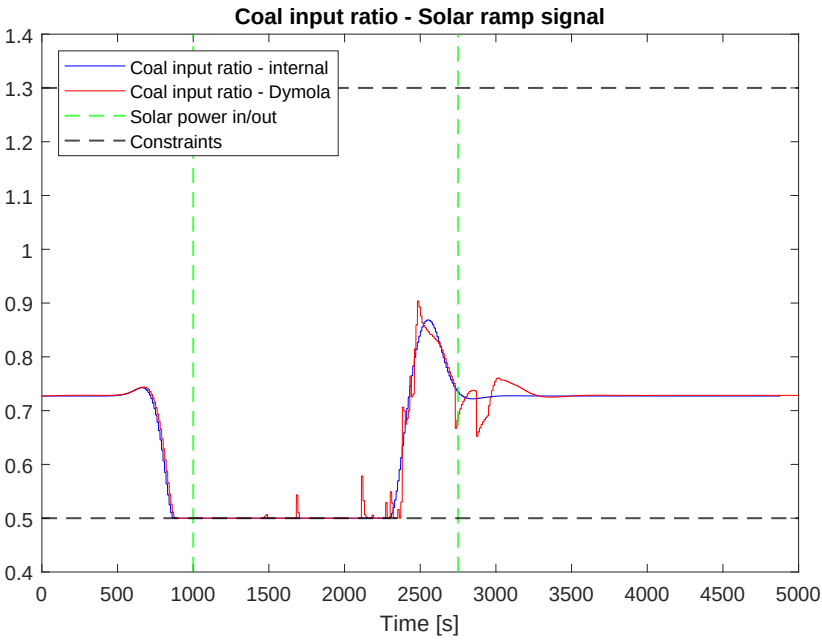

Figure 5.18: *Coal input ratio of both models.*

6

Discussion

By applying the simple modification of adding a delay factor to the PID controller it is possible to achieve significant improvements in the system's performance while stable and running under maximum efficiency. It is thus clear from both experiments that the PID controller with the delay modification performs better under different scenarios of solar power input - showing clear gains in its implementation for a real industrial plant.

A summary of the range of the total power volatility and the range of battery load volatility for the solar step experiment is presented in Table 6.1 and for the solar ramp experiment in Table 6.2. Table 6.1 reveals how both MPC structures perform better during the solar step experiment, both in terms of decreasing battery usage and total power volatility, than the PID controllers. However, for the solar ramp experiment, shown in Table 6.2, there is a marginal difference in the performance of the MPC controllers over the PID with the delay modification, in terms of total power volatility, the PID controller with the delay modification performs even better than the MPC controllers. The MPC controllers do not perform better than the base-line PID model in terms of power generation volatility, in which the base-line PID controller has a lower maximum than the MPC controllers. Noteworthy is that the MPC controllers perform very similarly. There

Table 6.1: *Volatility for solar step experiment.*

Control structure	$\min(SOC_{vol})$	$\max(SOC_{vol})$	$\min(P_{tot,vol})$	$\max(P_{tot,vol})$
PID	-69.4%	67.2%	-41.8%	41.4%
PID & delay	-19.8%	20.0%	-35.7%	25.0%
MPC internal	-6.66%	8.56%	-18.75%	14.61%
MPC Dymola	-6.04%	9.74%	-19.02%	15.09%

Table 6.2: *Volatility for solar ramp experiment.*

Control structure	min(SOC_{vol})	max(SOC_{vol})	min($P_{tot,vol}$)	max($P_{tot,vol}$)
PID	-31.1%	32.3%	-7.62%	7.17%
PID & delay	-5.61%	4.81%	-2.01%	1.93%
MPC internal	-2.80%	7.14%	-5.89%	8.54%
MPC Dymola	-2.23%	8.12%	5.93%	8.79%

is a marginal difference between the two implying that the modelling performs well in this aspect.

It is more difficult for the controllers to adapt to a rapid change in solar power: both PID controllers presented frequency ranges outside the constraints, and the volatility of all metrics, for all controllers, increased. However, it is noteworthy that real incoming solar power is more alike to a ramp signal than to a step signal: this yields a positive outlook for the performance of the controllers in a real-world application.

The volatility in the coal input ratio for the Dymola model is most likely due to modelling issues. While testing the optimizer under various cost functions, the volatility was still always present. This could be due to modelling issues within the coal boiler or as a consequence of the control delay implementation algorithm. It is difficult to test and pinpoint the cause of the volatility as the testing would require a new model of the coal boiler or test another control delay implementation algorithm, which due to time resources, cannot be implemented.

The instability of the frequency for the MPC controlling the Dymola plant is most likely due to modelling errors. Simulations were run multiple times with different values for the weighing of the frequency in the optimizer; yet the frequency always became unstable once the solar energy entered the model - implying that the optimizer settings are not the problem. Now, there is a factor of modelling components that could be modelled faulty; however, the most likely culprit is the turbine/generator component. As noted in Section 2.2, the turbine/generator has been linearized at 50 Hz. The linearization causes issues as the frequency steers away from 50 Hz, most likely causing instability. However, it is unclear what causes the initial shift from the linearization point. It is possible that the frequency deviation that occurs even when the MPC runs on its own model, see Figures 5.9 and 5.14, is enough to make the linearization unstable when in contact with the Dymola model which in turn makes the optimizer unable to find an optimum satisfying all constraints.

7

Conclusions

This thesis project aimed to investigate whether it is possible to predict incoming solar power and to adjust steam power production accordingly to decrease the volatility in total power generation. Furthermore, the thesis project aimed to evaluate the performance of various predictive control strategies against the baseline industrial PID control model.

This thesis project's findings prove that simple and complex control modifications are possible within the industrial complex, yielding the complex more adaptable to the introduction of solar power. The PID delay modification provides the industrial complex with a simple solution to greatly decrease the volatility of the total generated power and require a smaller battery - thus creating a more economically viable model as a larger battery yields significantly larger costs for a real-world implementation. The MPC controller also yields the industrial plant an improvement in the minimum volatility of its total power generation and a decreased use of the battery.

The PID with the delay modification performed better than the baseline industrial model in the two evaluating aspects: in decreasing the usage of the battery and in generating a constant power output. Additionally, the PID with the delay modification did not cause further instability as compared to the baseline model. The MPC controllers were not superior to the baseline model in all aspects. The MPC model performs better than the the baseline PID controller in dealing with a solar step, but performs slightly worse in the constant flow of energy power when the solar enters as a ramp; however, this is off-set by the significantly lower usage of the battery compared to the baseline model: a 91.0% and a 92.8% decrease for the MPC internal model and the MPC Dymola model respectively; in contrast, the power output volatility features a 19.1% and a 22.6% increase for the MPC internal model and the MPC Dymola model respectively. There is thus a trade-off in the usage of the battery and the consistency of the power output

when considering the baseline PID controller and the MPC controllers. Most crucially, however, is the instability generated by the MPC controller running on the Dymola model making it non-realistic in its current state.

Tt is unclear whether the step solar signal should be taken into account when evaluating the models. The step solar signal does reveal insight into the extreme cases in which the control structures may operate, however, solar power will not realistically enter the system with such intensity; analysing the work of this thesis for real-world application should therefore prioritize the findings of the solar ramp experiments over the solar step experiments.

In sum, the negative factor, and the strength, of the MPC is that it is model-based. The accuracy of the model is as such directly correlated to the controller's output and a miss-modelled plant can make the MPC structure unstable.

7.1 Future work

The development of the simulation environment proved to be more time-consuming than initially anticipated; as such with a finished simulation environment, more time can be allocated to fine-tuning the optimization parameters and the control structures presented in this thesis project.

With more time allocated to it, the issues presented in Chapter 6 would likely be solved and yield any future work improved performance and an increasingly accurate analytical framework for comparing the various control methods.

Improvements in the performance of the control models involve testing of different delay horizons for the PID controller and testing of various scaling factors for the coal input ratio. Further work within the MPC structure is approaching the modelling of the generator/turbine from another angle than through linearization. There is also a possibility that another type of MPC structure could yield significantly better performance than the MPC structure selected in this thesis project, as only one MPC structure was tested in this project.

Future work should also test various circumstances of the incoming solar power: how the controllers react to stochastic solar power and how the controllers react to disturbances and errors in the incoming solar power model.

Bibliography

[1] Abdul Afram and Farrokh Janabi-Sharifi. Theory and applications of hvac control systems–a review of model predictive control (mpc). *Building and Environment*, 72:343–355, 2014.

[2] Gholamreza Ahmadi, Davood Toghraie, and Omid Ali Akbari. Solar parallel feed water heating repowering of a steam power plant: A case study in iran. *Renewable and Sustainable Energy Reviews*, 77:474–485, 2017.

[3] Mohammad Reza Akhtari and Mehdi Baneshi. Techno-economic assessment and optimization of a hybrid renewable co-supply of electricity, heat and hydrogen system to enhance performance by recovering excess electricity for a large energy consumer. *Energy Conversion and Management*, 188:131–141, 2019.

[4] Ali Arzani and Ganesh K Venayagamoorthy. Computational approach to enhance performance of photovoltaic system inverters interfaced to utility grids. *IET Renewable Power Generation*, 12(1):112–124, 2018.

[5] Martin Behrendt. Mpc scheme basic. `https://commons.wikimedia.org/wiki/File:MPC_scheme_basic.svg`. Accessed: 2023-03-24.

[6] L Bigarelli, A Lidozzi, M Di Benedetto, L Solero, and S Bifaretti. Model predictive energy management for sustainable off-shore oil and gas platforms. In *2019 21st European Conference on Power Electronics and Applications (EPE'19 ECCE Europe)*, pages P–1. IEEE, 2019.

[7] Karl Johan Åström Bo Bernhardsson. Model predictive control (mpc). https://www.control.lth.se/fileadmin/control/Education/DoctorateProgram/ControlS Accessed: 2023-03-24.

[8] Rafael Celuppi, Jaqueline Scapinello, Felipe GD Andrade, Jaime HP Revello, and Jacir Dal Magro. Solar energy use for water pre-heating in boilers of agro-industries. *Engenharia Agrícola*, 34:451–460, 2014.

[9] Keh-Chin Chang, Wei-Min Lin, and Kung-Ming Chung. Solar water heaters as a pre-heating system for industrial processes. *Energy Efficiency*, 11:755–760, 2018.

[10] Xianzhong Chen, Mohsen Heidarinejad, Jinfeng Liu, and Panagiotis D Christofides. Composite fast-slow mpc design for nonlinear singularly perturbed systems. *AIChE Journal*, 58(6):1802–1811, 2012.

[11] Stefano Di Cairano, Daniele Bernardini, Alberto Bemporad, and Ilya V Kolmanovsky. Stochastic mpc with learning for driver-predictive vehicle control and its application to hev energy management. *IEEE Transactions on Control Systems Technology*, 22(3):1018–1031, 2013.

[12] Martin Enqvist. Industriell reglerteknik: Föreläsning 9. https://www.control.isy.liu.se/student/tsrt07/lecture/lecture09ho.pdf. Accessed: 2023-03-24.

[13] Yu Han, Yingying Sun, and Junjie Wu. A low-cost and efficient solar/coal hybrid power generation mode: Integration of non-concentrating solar energy and air preheating process. *Energy*, 235:121367, 2021.

[14] BS Hartono, Yan Budiyanto, and Rudy Setiabudy. Review of microgrid technology. In *2013 international conference on QiR*, pages 127–132. IEEE, 2013.

[15] Tor Aksel N Heirung, Joel A Paulson, Jared O'Leary, and Ali Mesbah. Stochastic model predictive control—how does it work? *Computers & Chemical Engineering*, 114:158–170, 2018.

[16] Adam Hirsch, Yael Parag, and Josep Guerrero. Microgrids: A review of technologies, key drivers, and outstanding issues. *Renewable and sustainable Energy reviews*, 90:402–411, 2018.

[17] IEEE. Ieee guide for using ieee std 1547 for interconnection of energy storage distributed energy resources with electric power systems. *4. General interconnection technical specifications and performance requirements [1547]*, 1547.9:17–30, 2022.

[18] Eric C Kerrigan and Jan M Maciejowski. Soft constraints and exact penalty functions in model predictive control. 2000.

[19] Jong S Kim, Kody M Powell, and Thomas F Edgar. Nonlinear model predictive control for a heavy-duty gas turbine power plant. In *2013 American control conference*, pages 2952–2957. IEEE, 2013.

[20] Basil Kouvaritakis and Mark Cannon. Model predictive control. *Switzerland: Springer International Publishing*, 38, 2016.

[21] Robert H Lasseter and Paolo Paigi. Microgrid: A conceptual solution. In *2004 IEEE 35th annual power electronics specialists conference (IEEE Cat. No. 04CH37551)*, volume 6, pages 4285–4290. IEEE, 2004.

[22] Lu Liu, Siyuan Tian, Dingyu Xue, Tao Zhang, and YangQuan Chen. Industrial feedforward control technology: a review. *Journal of Intelligent Manufacturing*, 30:2819–2833, 2019.

[23] MathWorks. fmincon. https://www.mathworks.com/help/optim/ug/fmincon.html, Accessed: May 13, 2023.

[24] Ryan McCloy, Lai Wei, and Jie Bao. A contraction-constrained model predictive control for multi-timescale nonlinear processes. *arXiv preprint arXiv:2205.04465*, 2022.

[25] Stephen Mills. Combining solar power with coal-fired power plants, or cofiring natural gas. *Clean Energy*, 2(1):1–9, 2018.

[26] Rodrigo Palma-Behnke, Carlos Benavides, Fernando Lanas, Bernardo Severino, Lorenzo Reyes, Jacqueline Llanos, and Doris Sáez. A microgrid energy management system based on the rolling horizon strategy. *IEEE Transactions on smart grid*, 4(2):996–1006, 2013.

[27] Kody M Powell, Khalid Rashid, Kevin Ellingwood, Jake Tuttle, and Brian D Iverson. Hybrid concentrated solar thermal power systems: A review. *Renewable and Sustainable Energy Reviews*, 80:215–237, 2017.

[28] Arthur Richards. Fast model predictive control with soft constraints. *European Journal of Control*, 25:51–59, 2015.

[29] Xinglong Zhang, Marcello Farina, Stefano Spinelli, and Riccardo Scattolini. Multi-rate model predictive control algorithm for systems with fast-slow dynamics. *IET Control Theory & Applications*, 12(18):2468–2477, 2018.